Delft University of Technology

Evaluation of Foam-Assisted Chemical Flooding at Reservoir Conditions

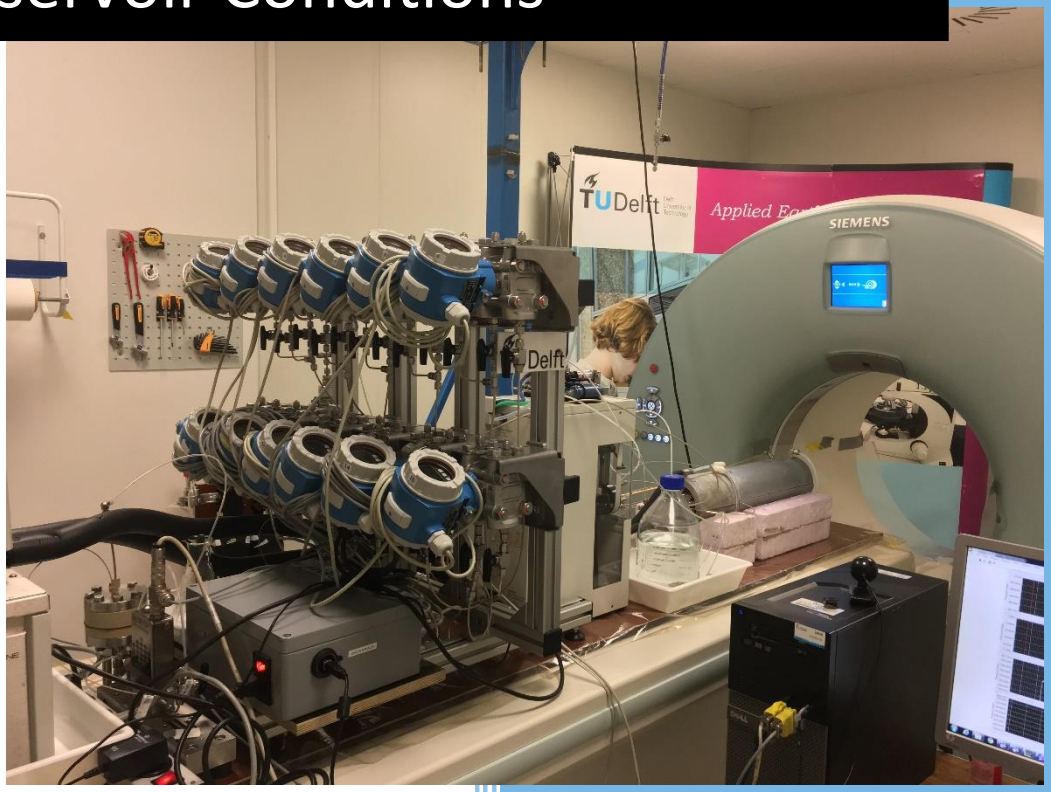

Abdulaziz Al Mutawa

4626443

TUDelft

Evaluation of Foam-Assisted Chemical Flooding at Reservoir Conditions

By

Abdulaziz Al Mutawa

in partial fulfilment of the requirements for the degree of

Master of Science

in Applied Earth Sciences

at the Delft University of Technology

to be defended publicly on Friday September 14, 2018

Student Number:	4626443	
Supervisors:	Prof. Pacelli Zitha	TU Delft
	Martijn Janssen	TU Delft
Thesis Committee:	Prof. Dr. Pacelli Zitha	TU Delft
	Prof. Dr. Bill Rossen	TU Delft
	Prof. Dr. Giovanni Bertotti	TU Delft
	Dr. Sebastien Vincent-Bonnieu	SHELL

Abstract

Despite recent drop in the growth of global oil demand, the trend is expected to gradually pick up and continue increasing. Industrial and transportation sectors are still considered the highest consumers of oil. The petrochemicals sector's demand for oil is increasing sharply and expected to continue in that fashion for the upcoming years. As oil fields age and mature, extraction of oil via primary and secondary techniques becomes, to an extent, inefficient. That encourages more research and development in enhance oil recovery (EOR) methods. In EOR, the aim is to either change a physical or chemical property of reservoir fluid in order to improve the oil recovery factor. The techniques can be categorized as thermal, physical, chemical or gaseous. In this experimental study, the lessons learned from gas flooding methods and surfactant flooding methods are taken into account in order to come up with a novel Foam-Assisted Chemical Flooding (FACF) procedure that aims to enhance the oil recovery factor to its maximum. In this approach, a surfactant slug solution is injected into a core at residual oil after water flooding conditions to mobilize trapped oil by capillary pressure. Then, a surfactant drive solution is co-injected with N_2 for foam generation to serve as mobility buffer displacing the accumulated mobilized oil. The experimental study is performed under reservoir conditions of 90 $\pm 1^{o}$C temperature and 20 bar of back pressure. In this study, surfactant stability is tested in synthetic formation brine. Then, phase behaviour tests are conducted to identify the capability of the surfactant to reduce o/w interfacial tension (IFT) to ultra-low values. The resulting solutions are categorized into their associated Winsor Types and classified based on salinity as under-optimum, optimum and over-optimum. A final surfactant slug solution is formulated based on these tests. Afterwards, bulk foam tests are performed in absence and presence of crude oil to test surfactant foaming ability and the resulting from stability and strength. Core-flood experiments are carried out to assess the possibility of generating foam in porous media in absence of crude oil and at residual oil to waterflooding. Full EOR FACF experiments are conducted, two at under-optimum and two at optimum salinity conditions. Two FACF experiments are performed with the assistance of medical CT scanner. In one FACF experiment, the foam is pre-generated utilizing a mixing tee and then injected into the Bentheimer sandstone. The study reported here showed that surfactants are not stable in synthetic seawater injection brine, as it tends to form complexes in presence of divalent ions, and subsequently generate precipitations. Stability was achieved by removing the divalent ions from the synthetic brine. In addition, phase behaviour study yielded that surfactant (A) is a better o/w IFT reduction agent than surfactant (B). A distinct layer of micro-emulsion was observed in excess of water and oil phases. On the other hand, surfactant (B) displayed better foaming abilities than surfactant (A) in absence of crude oil. Using surfactant (B), foam was generated in multiple qualities in a Bentheimer sandstone core-flood experiments in absence of crude oil. The critical foam gas fraction was found to be 75%. However, attempts to generate foam in porous media at residual oil to water flooding conditions were not successful. In three FACF core-flooding experiments, weak and unstable foam was generated during the surfactant drive co-injection phase. Whereas, in the last FACF experiment where a mixing tee was utilized, pressure drop and gas breakthrough data show that stable foam was generated. The CT images from two FACF experiments, one at optimum and the other at under-optimum salinity conditions displayed unstable water front in waterflooding phase, and unfavourable

mobility conditions, during the surfactant slug injection. However, the effect of salinity conditions was seen in the different oil bank shapes in both experiments. The one at under-optimum salinity condition showed more unstable front. The study reported here showed that the FACF technology yields improving oil recovery of 70±5%, 77±5% and 73±5% for the FACF experiments where it was very challenging to generate foam in-situ and reached up to 80±5% of oil initially in place in the case where foam was pre-generated outside the core (55%, 61%, 59% and 46% are the oil recovery factors after waterflooding, respectively). The study revealed that drive foam strength has a bigger impact than its surfactant slug salinity.

Acknowledgments

In the hope of developing myself further, I have been fortunate enough to receive Saudi Aramco Scholarship of Excellence to pursue an advanced degree in Petroleum Engineering at Delft University of Technology. Delft University of Technology offers one of the industry's most prestigious advanced graduate programs, the Masters of Science in Petroleum Engineering. The program incorporates a wide range of courses that cover petroleum engineering and earth sciences with practices and field work activities. The multidisciplinary group projects along with the individual exercises fit my personal and professional needs. As collaborative team projects are essential, the Masters of Science in Petroleum Engineering enhanced my ability to thrive in fast-paced environments while remaining focused on attaining objectives.

Focusing on the project that I present to you in this report, I was fortunate enough to have the chance to conduct multiple experiments at the Dietz laboratory in the faculty of Civil Engineering and Geosciences. I would like to extend my sincere thanks and appreciation to Professor. Pacelli Zitha, my supervisor, for granting me this opportunity. I would like to also thank him for sharing his knowledge, experience and valuable time throughout the entire thesis work.

As the experimental work requires daily extensive procedures, I would like to thank Martijn Janssen for his devotion and daily supervision throughout the entire experimental work. His continuous support, encouragement and guidance is highly appreciated.

Working in the Dietz laboratory throughout the project duration while conducting multiple experiments, wouldn't have been possible without the unlimited support by the technical staff, especially, Michiel Slob. His technical assistance with building the experimental setup and implementing the required procedures is greatly appreciated and valued.

This project is part of a two-year journey at TU Delft. I would like to extend my sincere thanks and appreciation to the entire group of professors who helped me throughout this journey.

This thesis was done as part of a collaboration between Delft Univesity of Technology, University Teknologi Petronas, Petronas and Shell. I am grateful to Petronas and Shell for funding the project, as well as for the supply of materials and data.

I would like to also thank the thesis committee members for their interest in my topic and for giving me the chance to defend my thesis in front of them.

Table of Contents

List of Tables

List of Figures

1 Introduction

1.1 General introduction

Oil is a valuable commodity that is considered a main component and source of energy in many sectors. The recent oil market reports show a continuous growth in oil demand globally (OPEC, 2018). The industrial and transportation sectors have been considered the main consumers of oil. However, nowadays, the growth in oil demand relevant to transportation is slowing down, and expected to continue following this trend in the future. On the other hand, the petrochemicals industry is now driving the demand growth in a fast manner (International Energy Agency, 2018). Residential and commercial sectors also contribute to the overall growth of the demand. Therefore, a continuous and timely supply of oil is very crucial to satisfy the international oil demand.

With the fluctuations in the financial markets and as the oil industry becomes more tumultuous, the need for research and development in finding new ways to extract oil from subsurface is at large. Oil producers aim at extracting the maximum amount of oil in a safe and efficient way. On the other hand, oil consumers look for a stable, continues and cost efficient supply. In that essence, academic participation in the research and development in the industry to come up with innovative strategies in oil extraction gains its importance.

1.2 Study background

Oil reservoirs go through a cycle. It starts with the exploration phase, then goes through the appraisal phase, and afterwards reaches the development and production phase. The last phase that reservoirs go through is abandonment. In every phase of the cycle sub-phases are present with multiple stages.

For any given field development plan, one of the important steps is to define the oil depletion plan and strategy. The recovery stages of oil are categorized into Primary, Secondary and Tertiary recovery. In primary recovery, the natural energy of the reservoir is considered as the drive mechanism by which oil flows to the surface. Whereas in the secondary recovery, it is supported by the injection of water or gas from surface. The main goal of injection in the secondary recovery is pressure maintenance. The tertiary stage includes variety of enhanced oil recovery (EOR) techniques that alters chemical or physical properties of reservoir fluids. EOR is an innovative topic in the oil industry. Multiple EOR methods have been applied in the industry varying in their associated cost, efficiency and applicability. Many of these methods

were proved to be effective in laboratory and in different fields and settings around the globe (Awan, 2008).

EOR methods can be classified into thermal, gaseous, chemical and physical processes. Every process has its sub categories. In this study, one of the chemical EOR processes is evaluated; an EOR technique that utilizes chemically formulated surfactant slugs (oil mobilization) and foam (mobility buffer).

The use of foam for mobility control in EOR is gaining a lot of attention from the industry and promises to overcome multiple drawbacks of the presently, often applied, gas flooding processes (Li, et al., 2010). Gravity override, channelling and early gas breakthrough, as well as viscous fingering are the main shortcomings of gas flooding injection methods (Rossen, 1996). Foam as a drive agent improves the volumetric sweep efficiency. With the ability of foam to significantly reduce gas mobility, it provides an improved mobility buffer between the injectant and the reservoir fluids in place, and consequently results in a more stable displacement of oil (Farajzadeh, 2015).

Besides using surfactants for foam generation, they are widely utilized in the industry in chemical flooding processes such as Alkali Surfactant Polymer (ASP) and Surfactant Polymer floodings. The surfactant in such techniques is employed to reduce the o/w interfacial tension (IFT) to ultra-low values. This contributes in mobilizing trapped oil and hence may reduce oil saturations in swept areas to below 1% of OIIP (Southwick, et al., 2018).

Foam-Assisted Chemical Flooding (FACF) is a novel EOR process that combines the use of surfactants, for trapped oil mobilization after water flooding, and for foam generation as a drive mobility. This includes the injection of a specially designed surfactant slug to mobilize residual oil saturation (sketch 2, in figure 1) and followed by co-injection of a specifically formulated surfactant drive solution with gas to generate foam for mobility control (sketch 3, in figure 1). This project aims to evaluate FACF at specific reservoir conditions.

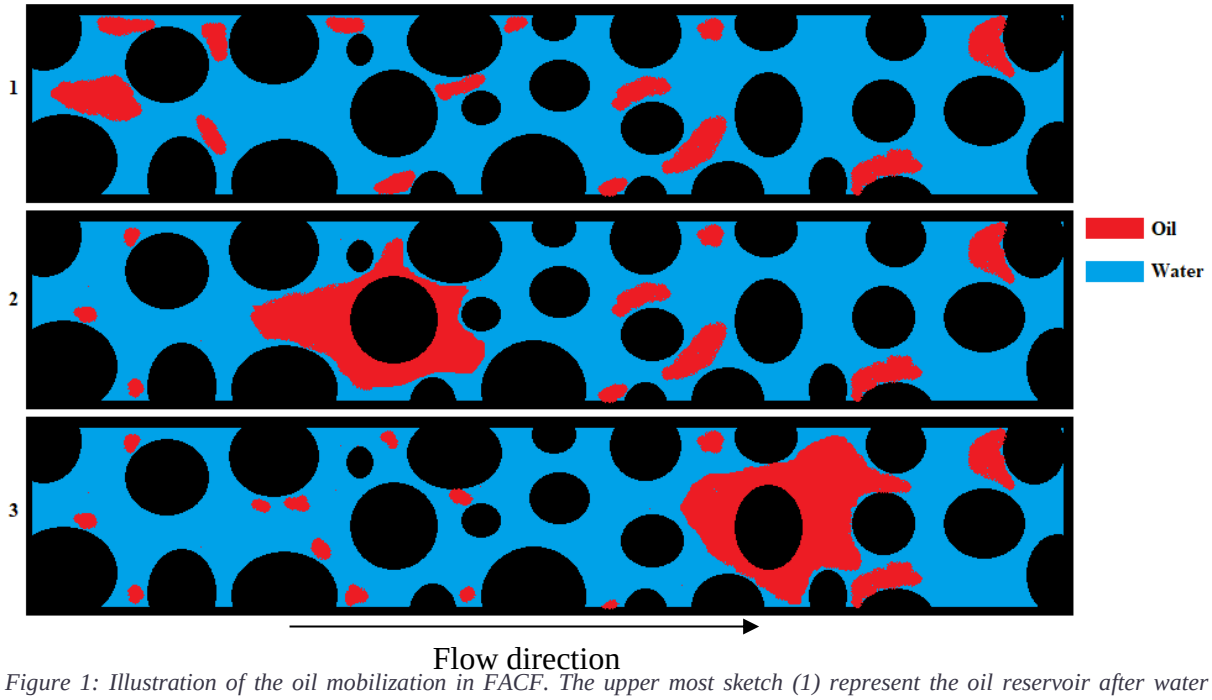

Figure 1: Illustration of the oil mobilization in FACF. The upper most sketch (1) represent the oil reservoir after water flooding, reaching a residual oil to water flooding condition (S_{or_WF}). The second sketch represent the situation after the injection of surfactant slug, which resulted in mobilizing trapped oil droplets, and oil accumulation crossed the first third of the core. The bottom most sketch (3) represent the situation during drive foam injection. It displaced the oil accumulation towards the end of the core for production..

1.3 Rationale

In the targeted field, primary and secondary recovery techniques yielded a recovery factor of 46% from stock tank oil initially in place (STOIIP). As the oil reservoir matures and ages, EOR processes become more appealing alternatives or complements to secondary recovery methods. In fact, the stakeholders are interested in implementing novel EOR techniques to improve the recovery factor to higher magnitudes. In a comprehensive EOR screening study conducted in 2000, it was shown that chemical, gas flooding and microbial EOR processes have the most practical aspect (Samsudin, et al., 2005). Chemical and gaseous EOR techniques such as Alkali-Surfactant (AS), Surfactant Polymer flooding (SP) and gas flooding have been studied in laboratories and successfully implemented in different fields globally (Samsudin, et al., 2005). However, such techniques have certain drawbacks. For gas flooding, disadvantages include gas override, gas channelling and viscous fingering. One of the important reasons leading to such shortcomings is the unfavourable mobility ratio between gas and oil/water, which consequently leads to poor sweep efficiency (Zitha, et al., 2018). On the other hand, the application of SP flooding and AS flooding in remote locations with space limitation is very challenging. That is for the associated cost of manufacturing, delivering and capabilities of storing the large quantities of chemicals and fluids to be used in these techniques (Southwick, et al., 2018).

From the above mentioned reasons, evaluating FACF process comes in interest. That is due to the fact that it combines the utilization of two concepts; injection of surfactant slug for oil mobilization and co-injection of a surfactant drive with gas for foam generation to displace oil. The use of foam as a drive reduces the required amount of chemicals compared to AS and SP flooding. The utilization of foam as a mobility drive in a chemical/surfactant flooding process could be considered as a relatively new find out. Recently conducted studies showed thath the use of such a drive in a surfactant flooding process may yield successful results (Srivastava, et al., 2009; Li, et al., 2010; Guo, et al., 2011). Several names were proposed for the process including Alkaline-Surfactant-Foam (ASF) flooding, Low Tension Gas (LTG) flooding and Alkaline-Surfactant-Gas (ASG) flooding. In this work FACF is adopted due to the absence of alkaline as an injectant.

1.4 Research Questions

The aim of this research is to study the optimization and the efficiency of the FACF technique at reservoir conditions. Bentheimer sandstone cores were used as a model reservoir due to its homogeneous mineralogy and fairly high permeabilities. The study was conducted under reservoir conditions with a temperature of 90 ±1^{o}C, while utilizing original brine composition and crude oil. Optimization was assessed in the context of the amount of produced clean oil-emulsified oil ratio, surfactant slug salinity and the displacement behaviour of the mobilized oil bank by foam.

In this work, a systematic experimental study based on multiple (CT-assisted) core-flood experiments, along with dedicated bulk foam and phase behaviour tests are reported.

The following research questions are addressed in this project:

- Are the surfactants assessed stable in the presence of injected seawater?
- How does surfactant A compares to surfactant B in terms of foaming capacities and foam stability in bulk?
- How does surfactant A compares to surfactant B in terms of o/w IFT reducing capacity?
- How does the salinity of the surfactant slug affect the dissemination of oil bank and the produced clean oil-emulsified oil ratio?
- Is the surfactant selected as a foaming agent potent enough to displace the mobilized oil bank efficiently?
- How does the injection of pre-generated foam influences the displacement of the oil bank?

1.5 Study approach

This is an experimental project involving phase behaviour experiments, bulk foam tests and multiple core-floods, two of which are medical CT-assisted. Since this experimental project is done under reservoir conditions, brine was prepared to mimic injected seawater composition and ionic strength. The prepared solution is then tested for its stability by exposing it to a temperature of 90 ±1^{o}C. Based on the stability conditions, the composition of brine is modified to ensure no precipitation is yielded in the presence of surfactants.

Afterwards, with the resulting synthetic brine composition, phase behaviour tests were carried out to conclude which of the two surfactants studied is potent enough to serve as o/w IFT lowering agent. In this process, multiple test tubes were filled with equal volumes of aqueous solutions compromising of equal concentrations of surfactant solution and brine with different salinities, as well as equal volumes of oil. Then the test tubes are placed in the oven under a temperature of 90 ±1^{o}C and monitored on daily basis until equilibrium is reached. The solubilisation ratios are then calculated, and with Huh's empirical correlation oil/emulsion and water/emulsion IFT values are estimated (Sheng, 2011). With the visual observations along with the estimated IFT values, the test tubes with their different salinities are classified based on their associated Winsor type (II-, III or II+). Figure 2 presents the different Winsor types and the associated o/w IFT's (Sheng, 2011). It provides a clear distinction between under-optimum, optimum and over-optimum salinity regions. Phase behaviour tests will lead to choosing surfactant slug composition to be utilized in the core-flood experiments. With the identification of the surfactant to be used as an IFT lowering agent, additional steps are needed to select the best foaming agent among the available two types of surfactants.

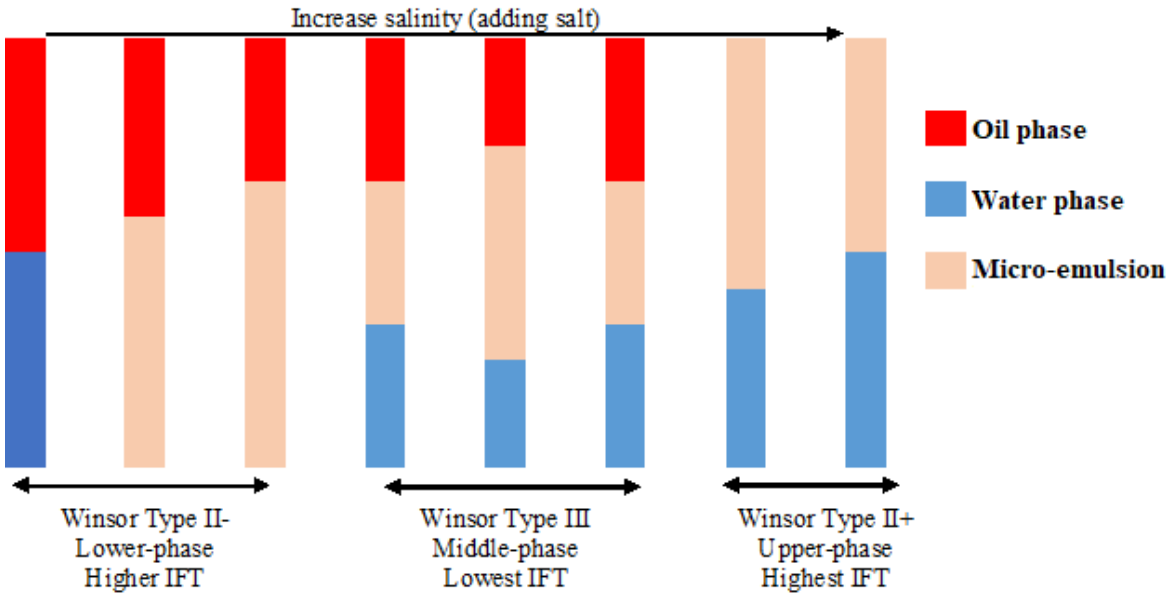

Figure 2: Different Winsor Types and associated o/w IFT's (Sheng, 2011)

To this end, several bulk foam tests are conducted both in the presence and absence of crude oil. In these tests, the surfactants solutions, consisting of surfactant dissolved in model brine, are placed in cylindrical tube with nitrogen gas (N_2) flowing through the solution from the bottom. Once foam column reaches a fixed volume the gas injection is shut off and foam stability is monitored as function of time. Afterwards, a comparison between the foams, using different surfactants, is applied. The more stable foaming agent is then tested for its capability to generate foam in the presence of crude oil. In this step, the effect of crude oil to the generation and stability of foam is studied. Eventually, the bulk foam experiments result in a surfactant solution to be selected as a drive solution.

Given that the surfactant selected for drive solution was able to generate stable foam in bulk, the next step is to investigate whether it can generate a strong and stable foam in porous media. Firstly, the selected surfactant is utilized to generate foam in a Bentheimer sandstone core in the absence of crude oil. Various foam qualities are tested in porous media; foam quality scan gives information on foam strength as function of gas fractional flow (Hua Guo, 2011). Subsequently, at a pre-determined foam quality, the foaming agent is examined for its ability to generate foam at residual oil to waterflood in a Bentheimer core.

With the model brine, surfactant slug and surfactant drive compositions determined, we have all of the ingredients to perform full FACF core-flood experiments. Four FACF EOR experiments were conducted, two of which at under-optimum salinity conditions (figure 2) and the other two at optimum salinity conditions. In the last experiment a mixing tee (i.e. foam

generator) was installed to the experimental setup to mimic a situation where foam is pre-generated and subsequently injected into the reservoir. An illustration of the study approach is presented below on figure 3.

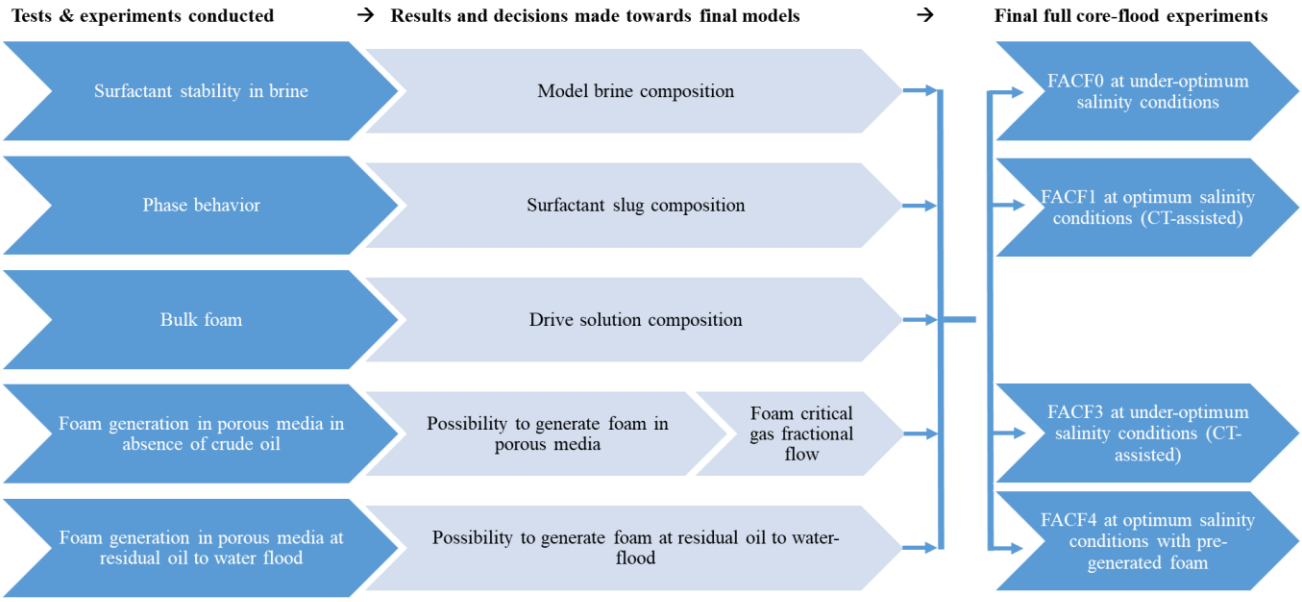

Figure 3: Study approach illustration

1.6 Ethical issues

As this study is performed as part of an integrated research project with Shell, Petronas and University Teknology Petronas, data related to the employed surfactants and the fields associated with the study are confidential.

1.7 Report structure

The report is structured in an order to ensure clarity and conciseness . It consists of six chapters: introduction, theoretical background, materials and methods, results and discussion, general discussion, and ends with the conclusions. The report started with a general introduction about the oil industry and the relevance of the study to the current and future market. Then, the geological setting of the targeted field was presented with the important characteristics and parameters. Afterwards, a background information about the EOR techniques, in general, and the FACF, in specific, were lightly explained with the motivation behind choosing this novel methodology. The research questions were laid out along with the study approach and the ethical issues concerning this study. In this chapter as well, the data and software employed throughout the study will be presented. In the upcoming chapters and sections more details will

be offered and discussed as we go further. In the theoretical background chapter, a thorough review of previous studies and literature concerning surfactants and foam in EOR processes will be discussed. The mechanism by which surfactants reduce o/w IFT will be explained, as well as Winsor type systems. In addition, light will be shed on foam in regards to its role in displacing oil and issues surrounding its strength and stability. The following chapter will show the materials and methods. It consists of five sections: chemicals, cores samples, experimental setup, medical CT-scanner and experimental procedures. The specifications and properties of all chemicals and core samples used in this study will be presented. A sketch of the experimental setup with a detailed explanation of every item will follow. Moreover, the CT-scanner specifications will be offered along with a justification of employing it in the core-flood experiments. Then, in the experimental procedure, the way by which all of the tests and experiments were conducted will be shown. Starting from the surfactant stability in brine, then bulk foam, followed by phase behaviour tests, the core-flood experiments afterwards and the CT data processing will end this chapter. In the results and discussion chapter, results will be viewed and discussed in the same previously mentioned chronological order. As of the results for the core-floods experiments, it will be presented with respect to the different injection stages for all core-floods. It will start with primary drainage and imbibition laying out the pressure drop data and CT images for all core-floods. Then, in the same fashion, information related to oil mobilization (i.e. slug injection) and oil displacement (i.e. drive co-injection) are showed and discussed. The following chapter lays down the general discussion in regards to the overall results of the different stages of the various core-flood experiments. Finally, in the conclusions chapter, the research questions are answered, and recommendations for future work are given.

1.8 Data and software

In this section, the sources of the acquired data and the different software programs accessed for data analysis will be presented. The data concerning the geological setting, formation brine, injection brine, and crude oil composition, was received from Petronas. For gas mass flow meter settings, a Matlab (R2018a for academic use) code was run to get the corrected gas flow rate, for the drive foam phase (i.e. the drive co-injection). In addition, ImageJ was used for visualizing and processing acquired CT-images.

2. Theoretical Background

2.1 Oil mobilization

An oil bank is an accumulation of mobilized oil, mobilized oil droplets/ganglia may coalesce to form an oil bank. It is the part of a reservoir where the saturation of the oil increases due to the application of EOR methods (Saraji *et al.,* 2013). The formation of the oil bank is necessary since it facilitates the collection of oil. In the absence of any oil bank, oil production will still be possible, however, it will be produced in a discontinuous way (slugs), which is not efficient. A key parameter to form a stable oil bank is coalescence, the build-up process of oil bank. Its prevents the oil bank form breaking down and stops isolated oil ganglia from re-entrapment (Al Saadi, Wolf, & Van Kruijsdijk, 2018). A number of physical and chemical factors that influence the formation and build-up of the oil bank are discussed in the following sections.

The capillary number - The capillary number (***Nc***) is the measure of the comparative outcomes of the action of viscous forces and surface/interfacial tension forces that acts between the liquid and gas interface or between two immiscible liquids (Salager *et al.,* 2013).

$$N_c = \frac{u\mu}{\sigma} \qquad \textit{Equation 1}$$

where u is the superficial velocity, σ is the IFT and μ is the viscosity of the wetting phase. N_C is inversely proportional to the IFT between any two different phases. That is when the IFT increases, N_C decreases and vice- versa. The role of the surfactant here is to reduce the o/w IFT, thus increasing N_C. In order to capture the process, a key surfactant property needs to be defined; the critical micelle concentration (cmc). The cmc is a concentration above which miscelles form, and additional concertation of surfactant goes to micelles. (Hanamertani, Pilus, Manan, & Ahmed, 2018).

Another important measure that plays a significant role in the capability of a surfactant to lower an o/w IFT is the aqueous salinity. It is related to the Winsor types (figure 2) created as a result of the salinity of the effect of solution on the amount of phases that are in equilibrium for a specific water-surfactant-oil system. The three Winsor types II(-), III, and II(+) are correlated with an optimum, under-optimum and over-optimum salinity range. The defining factor of these ranges is the point at which a distinct micro-emulsion phase is clearly present yielding an equilibrium between three phases. This corresponds to Type III Winsor system where an ultra-low o/w IFT is achieved, characterized by an oil/water micro-emulsion in presence of excess oil and water. On the other hand, for under-optimum and over-optimum salinities, an oil-in-

water micro-emulsion co-exists with additional oil (TypeII(-)), and a water-in-oil micro-emulsion co-exists with additional water (Type II(+)), respectively.

2.2 Oil displacement

Displacement efficiency of any oil bank is associated with the mobility ratio between the oil in place and the drive. The key factor is to achieve favourable conditions during the oil displacement process. That is possible when the displacing fluid has a lower mobility than the displaced fluid (Sheng, 2011). For a single phase, the mobility ratio can be simply represented as in the following equation:

$$\lambda = \frac{k}{\mu} \qquad \textit{Equation 2}$$

where λ is the mobility of the phase, k is the effective permeability and μ is the viscosity of the phase (Sheng, 2011). So, for any given fluid, as its viscosity decreases, its mobility increases. An increase in permeability constitutes an increase in mobility, as well. When a mobile fluid is displaced by another fluid, the process can be represented in having an upstream phase and downstream phase. The defining parameter to achieve an improved sweep efficiency is that the displacing phase upstream has a mobility value lower than or equal to the mobility of the displaced phase in the downstream (Sheng, 2011). With such conditions, the resulting mobility ratio between the displacing phase and the displaced phase will satisfy the favourable displacement condition; that is a mobility ratio less than or equal to one. The formula of mobility ratio is as follows:

$$M = \frac{\lambda_{upstream}}{\lambda_{downstream}} \qquad \textit{Equation 3}$$

where M is the mobility ratio, λ is the mobility of the phase (Sheng, 2011). In polymer flooding, for instance, polymers are used to increase the viscosity of the displacing phase. As in Equation 1, this will lead to the reduction of the mobility of the associated upstream phase. Hence, decreasing the value of mobility ratio. Figure 4 shows a comparison between the macroscopic displacement efficiency of oil by waterflooding and polymer flooding. It clearly shows that an improved displacement efficiency is achieved by polymer flooding.

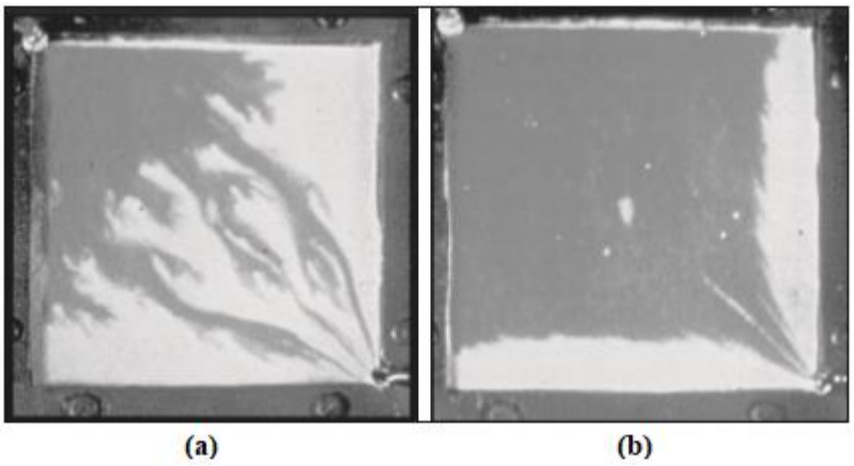

Figure 4: Macroscopic displacement efficiency: (a) water flooding, (b) polymer flooding (Sheng, 2011)

This emphasises the importance of mobility control process in EOR techniques, especially chemical EOR methods. In addition to mobility ratio, among the factors that affect oil bank displacement are rock porosity and permeability properties, o/w IFT, salinity of the surfactant slug solution and accessible pore volume (Al Saadi, et al., 2018).

Foam is defined as "dispersion of gas in liquid such that the liquid phase is interconnected and at least some of the gas flow paths are blocked by lamellae" (Rossen, 1996). Lamellae is a thin liquid film. Lawson and Reisberg introduced foam as a mobility control agent in surfactant flooding in 1980 (Li, et al., 2010). However, what prevented the immediate implementation of this idea is that the mechanism by which foam functions as a mobility control agent was vague. The study of steam foam process mechanisms by (Hirasaki, 1989) and the work of (Patzek, 1996), along with the successful field tests such as the one carried out on Snorre field in North Sea, helped in drawing a better picture to understand the mechanism by which foam serves as mobility control agent (Li, et al., 2010). One component in that picture was the conclusion that in order for foam to generate in porous media, it has to exceed the critical pressure gradient (Falls, et al., 1988; Rossen, 1996; Kam & Rossen, 2003). It is a point below which the continuous flowing phase is gas with very low mobility reduction, and above which foam exists, in the shape of bubbles (Li, et al., 2010). In addition, it was understood that the stability of the lamellae is affected by N_C. A critical capillary number below which bubbles of gas/liquid start to coalesce, creating an unstable condition (Li, et al., 2010). So, in order to have a stable foam films, surfactants are applied. The adsorption of the surfactant at the gas/liquid interface makes them more stable (Rouhi Farajzadeh, 2009). Foam is generated in porous media via co-injection of gas and surfactant solution, surfactant-alternating-gas (SAG) injection, or by dissolving the surfactant in the injected gas (Rouhi Farajzadeh, 2009).

2.3 FACF

FACF is a process that associates the use of a specifically designed surfactant slug to mobilize water flooded trapped oil ganglia by reducing the o/w IFT. Subsequently, it employs foaming as a mobility buffer to displace the mobilized/accumulated oil in order to be produced. Previous studies and experiments conducted show a significant increase in oil recovery due to such process (Janssen, et al., 2018; Guo, et al., 2011). Both studies have shown that the utilization of surfactant slug as an agent to lower o/w IFT (pre-flush), followed by foam flooding as a mobility drive process resulted in a significant improvement in recovering oil left behind after water flooding. The benefits of having foam as a mobility drive over polymer is the temperature limitations of polymers as it degrades at elevated temperatures. Furthermore, polymers cannot be utilized at high salinities as high salt concentrations degrade their viscosity (Pal, et al., 2017). Moreover, lots of commercial polymers cannot be employed in low permeability reservoirs (Shupe, 1981). In addition, given that the largest volume contribution in generating foam comes from gas, it reduces the space limitation required to store materials/chemical, in comparison to polymers, and reduces associated costs.

3. Materials and Methods

3.1 Chemicals

In this experimental study, multiple chemicals were utilized. Table 3 provides an overview and summary of all of the chemicals with their associated properties. Sodium Chloride (NaCl), Sodium Carbonate (Na_2CO_3), Potassium Chloride and Sodium Sulphate (Na_2SO_4) were dissolved in demineralized water for synthetic brine preparation. The Sec-butanol ($C_4H_{10}O$) was used as a co-solvent in the surfactant slug solution. In order to enhance the CT contrast between aqueous and oleic phase, 1-Iododecane ($CH_3(CH_2)_9I$ was used as a dopant for the oleic phase. Surfactants A and B were supplied by Shell and Petronas, respectively, to be utilized in this experimental study for foam generation and o/w IFT reduction.

Table 1: Properties of chemicals used throughout the experimental study.

Chemical	**Formula**	**Molecular Weight [g/mol]**	**Density [g/cm^3]**	**Viscosity [mPa.s]**	**Purity [%]**
Sodium Chloride	NaCl	58,440	2.160 ±0.001	-	≥ 99
Sodium Carbonate	Na_2CO_3	105,990	2.540 ±0.001	-	≥ 99
Potassium Chloride	KCl	74.550	-	-	≥ 99
Sodium Bicarbonate	$NaHCO_3$	84.010	-	-	≥ 99
Sodium Sulphate	Na_2SO_4	142.040	-	-	≥ 99
Sec-butanol	$C_4H_{10}O$	74.120	0.806 ±0.001	-	≥ 99
1-iododecane	$CH_3(CH_2)_9I$	268.180	1.257 ±0.001	-	≥ 98
Surfactant A[a]	-	-	0.996 ±0.001	-	19
Surfactant B[b]	-	-	1.020 ±0.001	121.200	20
Nitrogen	N_2	28.010	1.165 ±0.01	1.760 ±0.005	≥ 100

a: surfactant A was supplied by Shell, b: surfactant B was supplied by Petronas

3.2 Core samples

In this work, Bentheimer sandstone cores were utilized to perform the core-flood experiments. The 40.00 cm length cores were drilled from a block coming from a sandstone outcrop. The sandstone is relatively clean with 91.00 weight percent (wt%) Quarts and categorized with relatively high permeability (Peksa, et al., 2015). The samples were then trimmed to the

required diameter by diamond saw. Placed in the oven at 60^{o}C to dry out for 48 hours, the samples are then glued with two layers of Epoxy resin grey glue so it can withstand a temperature of 90^{o}C. In order to measure pressure drop values along the core samples, multiple holes were drilled. The porosity was measured by CT scans and from the available literature (Peksa, et al., 2015). Whereas the permeability was estimated by applying 1-D Darcy equation with different flow rates while recording the pressure drops (Darcy, 1856). The properties of the Bentheimer sandstone cores are summarized in the table below.

Table 2: Bentheimer sandstone core samples properties

Parameter	**Core flood***	**FACF0**	**FACF1**	**FACF2**	**FACF3**
Porosity [%]	23.00 ±0.003	23.00 ±0.003	23.00 ±0.003	23.00 ±0.01	23.00 ±0.003
Permeability [Darcy]	3.42 ±0.20	2.48 ±0.50	3.73 ±0.30	3.58 ±0.80	3.76 ±0.20
Length [cm]	40.00 ±0.10	40.00 ±0.10	40.00 ±0.10	40.00 ±0.10	40.00 ±0.10
Diameter [cm]	3.80 ±0.10	3.80 ±0.10	3.80 ±0.10	3.80 ±0.10	3.80 ±0.10
Pore volume [cm^3]	104.34 ±7.27	104.34 ±7.27	104.34 ±7.27	104.34 ±10.63	104.34 ±7.27

*Core flood: this core sample was used twice; the first time for foam generation in porous media in absence of crude oil. After cleaning the core, it was used for foam generation at residual oil to waterflooding conditions. The reported permeability was measured before the first test for foam generation in porous media in absence of crude oil.

3.3 Experimental set-up

The experimental set-up for the core-flood experiments is illustrated in a schematic overview in figure 4. It consists of a core holder made of polyether ether ketone (PEEK) with a low X-ray attenuation and high mechanical strength, connected to a dual cylinder Quizix QX-6000 liquid pump used for the injection of aqueous solutions. In the case of crude oil injection, an additional vessel was utilized and connected to the liquid pump. Multiple pressure differential pressure transducers were used to monitor the pressure drop within the system throughout the different stages of the experiments. A backpressure regulator is connected to the outlet controlling the outlet pressure. To accurately estimate the breakthrough times of water, oil and

gas, a Coriolis flow meter was positioned at the outlet section of the set-up. For gas injection, N_2 was supplied from a 200 bar cylinder connected to the inlet via a mass flow controller (Bronkhorst). To record pressure and temperature behaviours, a data acquisition system was connected to a PC which recorded data using a time interval of 5 seconds. For the last experiment, a mixing tee (i.e. foam generator) was placed before the inlet section of the core-holder to pre-generate foam. The static mixing tee was installed before the core inlet section. It has two inlets, one for gas and the other for liquid, and an outlet where the mixture leaves the tee. All of the experiments were conducted under reservoir conditions of 90 ±1°C and 20 bar back pressure.

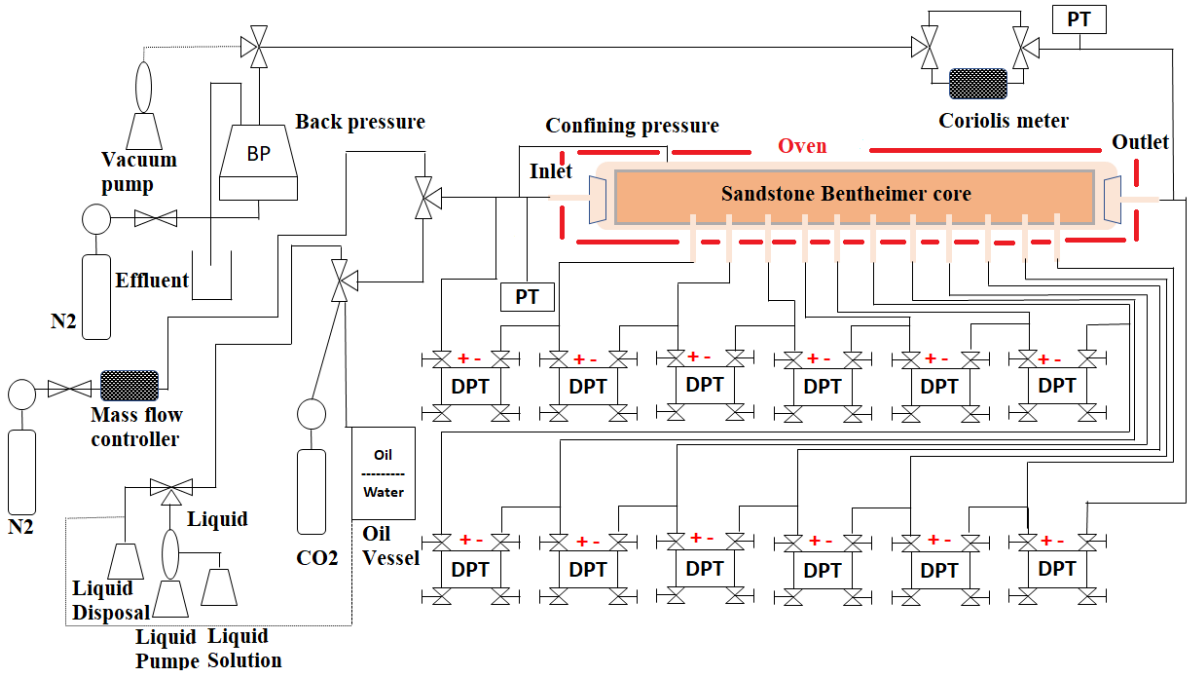

Figure 5: An illustration of the experimental setup on the bench. Similar setup was utilized at the CT scanning room. However, for heating, silicon heated sleeves were used to provide the required temperature of 90°C.

3.4 CT-scanner

In two of the performed experiments, a medical CT scanner was employed. The scanner uses simultaneous two X-ray tubes: 80 KeV voltage and 550 mA current, and 140KeV voltage and 250 mA current. A single scan consists of 270 slices of each 2 mm thick. The scanning process was performed in a spiral mode. In terms of accuracy, for two-phase condition while applying 140 KeV data, measured saturation had ±4% error. For three-phase condition, both 80 KeV and 140 KeV were used yielding a ±8% error in obtained saturations. The analysis and

visualization of CT scan data were done using ImageJ software. Table 5 summarizes the CT-scan settings.

Table 3: CT-scanner settings

Tube voltage	**[KeV]**	**80**	**140**
Tube current	**[mA]**	**550**	**250**
Slice thickness	**[mm]**	**2**	
Pixel size	**[mmxmm]**	**0.2 x 0.2**	
Scan mode		**Spiral**	

3.5 Experimental procedure

3.5.1 Surfactant stability in brine

The core-flood experiments in this study are planned to be carried out under reservoir conditions (90±1^{o}C and 20 bar back pressure). Therefore, it is important to evaluate the surfactant stability in brine. The injection seawater consists of NaCl, KCl, Na_2SO_4, $NaHCO_3$, $MgCl_26H_2O$ and $CaCl_22H_2O$. The different components of injection seawater were dissolved in demineralized water. Equal volumes of the prepared solution were poured into two test tubes. Afterwards, each surfactant of the available two was added to one tube. Later, the tubes were placed in oven under a temperature of 90±1^{o}C, and monitored on daily basis. Another solution was prepared to mimic the injection seawater, without divalent ions. This was to evaluate the effect of the presence of divalent ions on the stability of surfactants. In addition, another brine solution was prepared with the full composition, except for the $NaHCO_3$. This was also to study the effect that this component has on the solution itself and the surfactant stability. All tubes were placed in oven to satisfy the reservoir temperature and monitored on daily basis. Based on the stability conditions, the composition of brine was modified to ensure no precipitation is yielded in the presence of surfactants.

3.5.2 Phase behaviour

Salinity scans were conducted to assess salinity ranges of various potential surfactant slug formulations. Eventually, the goal of these scans is to determine the final surfactant slug formulation that will be used in the core-flood experiments. Multiple surfactant, brine and crude oil combinations were prepared with varying salinity range from 0 to 5 wt% of NaCl and KCl. The reason that both NaCl and KCl concentrations were altered is that we only wanted to change the total amount of monovalent chloride ions. The other components were kept constant consisting of crude oil at 1:2 oil-to-water ratio, 0.30 wt% surfactant (A or B), 1.00 wt% sec-

butanol, 0.37 wt% Na_2SO_4, and 0.32 wt% $NaHCO_3$. The prepared tubes were manually shaken for a period of three to five minutes, then placed on a shaker for a total duration of 10 hours. Afterwards, the tubes were placed inside an oven with a temperature of 90 ±1°C and monitored on daily basis until equilibrium was reached after two weeks. After equilibrium, it is ensured that no further micro-emulsion is being formed, or water going into oil phase and vice-versa. From this test, the amount of oil and water that went into micro-emulsion was measured. Then, the solubilisation ratios were estimated by applying Huh's empirical formula to estimate the oil/micro-emulsion and water/micro-emulsion IFT values (Lake, 1989). In addition, the different salinity regions corresponding to the different Winsor Type systems were identified in this test.

3.5.3 Bulk foam stability

Foam Scan instrument (I.T. Concept-TECLIS) was utilized in order to analyse foam generation and stability for both surfactant solutions A and B in absence of oil at room temperature of 20 ±1 °C and atmospheric pressure. In these tests, the surfactants solutions, consisting of surfactant dissolved in model brine, are placed in cylindrical tube with nitrogen gas (N_2) flowing through the solution from the bottom. Once foam column reaches a fixed volume, the gas injection is shut off and foam stability is monitored as function of time. Afterwards, a comparison between the foams, using different surfactants, is applied. Eventually, the goal is to select the final surfactant solution for foam drive.

3.5.4 Core-flood experiments

A total of six core-flood experiments were conducted. All of the core-flood experiments were performed on Bentheimer sandstone cores that have been fully saturated with brine. For the first experiment, the aim was to study the possibility of generating a stable foam in porous media in the absence of oil using the final surfactant drive formulation (the result from bulk foam stability tests). The second core-flood was performed on the same core at residual oil saturation to waterflood (S_{or_WF}): is it possible to generate foam at residual oil to waterflood (S_{or_WF}). The other four core-flood experiments were considered full EOR experiments. In these experiments, after primary drainage and water flooding processes, approximately 0.5 PV of surfactant A slug was injected to mobilize water flooded trapped oil prior to the co-injection of the selected surfactant B drive solution with N_2. Surfactant A and B were respectively chosen as the o/w IFT lowering agent and the foaming agent as a result of phase behaviour and bulk foam tests. Given that the S_{or_WF} is trapped by capillary forces, the injection of the surfactant

slug will effectively lower o/w IFT, mobilizing part of this trapped oil. Afterwards, N_2 was co-injected with the chosen surfactant drive solution (surfactant B) for displacement of oil bank. For the FACF1 and FACF2 experiments, a 20 wt% of 1-iododecane dopant was added to the crude oil, to enhance CT contrast between water and oleic phases. Without the dopant the CT response of theses phases are too close to each other and distinguishing between water and oil becomes nearly impossible. In the last experiment FACF3, 20 wt% of 1-iododecane dopant was added to the crude oil, not to enhance CT response (CT-scanner was not applied here). However, it was added to compare both experiments FACF1 and FACF3, so that the mixing tee (i.e. foam generator) was the only variable.

Table 4: Summary of core-flood experiments performed

Experiment	Procedure	Salinity range	Foam quality [%]	Dopent	CT-assisted	Mixing tee
Core-flood 1	Foam generation	-	Multiple	No	No	No
Core-flood 2	Foam generation at S_{or_WF}	-	57.5	No	No	No
FACF0	FACF	Under-optimum	57.5	No	No	No
FACF1	FACF	Optimum	57.5	Oil with 20 wt%	Yes	No
FACF2	FACF	Under-optimum	57.5	Oil with 20 wt%	Yes	No
FACF3	FACF	Optimum	57.5	Oil with 20 wt%	No	Yes

The sequence of the experimental procedure is similar in all of the core-flood experiments. Starting by flushing the core with CO_2 at an injection pressure of 5 bar for over two hours to ensure removal of all air from the core. Afterwards, the system is vacuumed. Then, the core was saturated with brine (approximately 10 PV) while a back pressure of 25 bar was applied to the system. The absolute permeability was measured by changing the flow rate utilizing Darcy's law (Darcy, 1856). Primary drainage followed. With that, 3 to 5 PV of crude oil was injected into the core at rate of 0.50 cm^3/min. After 2 PV of oil is injected and pressure has stabilized, a bump flood was performed (4.00 cm^3/min) to establish connate water saturation (S_{wc}). By varying the flow rates, the oil end-point relative permeability (k_{ro}^*) was estimated

using Darcy's law. Water flooding was then performed by injecting nearly 7 PV at a rate of 0.25 cm^3/min. As no oil was being produced after a specific PV of brine, and with the pressure stabilized, bump flood was performed to establish S_{or_WF}, as well as to overcome capillary end effect. Water end-point relative permeability (k_{rw}^*) was estimated using Darcy's law. With S_{or_WF} reached, the chosen surfactant slug solution (surfactant A) was injected to a total of 0.50 PV at a rate of 0.15 cm^3/min to mobilize S_{or_WF}. Finally, co-injection of N_2 and surfactant B drive solution was initiated to generate foam and displace the oil bank.

Table 5: Steps followed during core-flood and FACF experiments

Step	Experiment	Description	Back pressure [bar]	Flow rate [cm^3/min]
1	All	CO_2 flushing	-	-
2	All	Vacuuming	-	-
3	All	Brine saturation	25	0.25
4	Core-flood2, FACF0, FACF1, FACF2, FACF3	Oil injection	20	0.5
5	Core-flood2, FACF0, FACF1, FACF2, FACF3	Water flooding	20	0.25
6	FACF0, FACF1, FACF2, FACF3	Surfactant slug solution injection	20	0.15
7	Core-flood2, FACF0, FACF1, FACF2, FACF3	Surfactant drive co-injection	20	Liquid 0.2125 / Gas 3.732

The co-injection was continued until no further oil was produced. The core-flood experiments were analysed by the recorded and measured pressure drop data, relative permeabilities, mobility ratios, constructed recovery factors and clean-to-emulsified produced oil ratio. A summary of the physical properties of all fluids applied in these full EOR experiments is listed in table 8.

Table 6: Physical properties of all liquid phases used for conduction core-flood and FACF experiments

		Core-flood1	Core-flood2	FACF0	FACF1	FACF2	FACF3
Brine Salinity		1.75 wt% [NaCl + KCl]	1.75 wt% [NaCl + KCl]	1.00 wt% [NaCl + KCl]	1.75 wt% [NaCl + KCl]	1.00 wt% [NaCl + KCl]	1.75 wt% [NaCl + KCl]
Brine density	[g/cm^3]	1.0145 ±0.001	1.0145 ±0.001	1.0097 ±0.001	1.0145 ±0.001	1.0097 ±0.001	1.0145 ±0.001
Brine viscosity	[mPa.s]	0.36 ±0.05	0.36 ±0.05	0.38 ±0.05	0.36 ±0.05	0.38 ±0.05	0.36 ±0.05
Oil type		-	Crude Oil	Crude Oil	Crude Oil	Crude Oil	Crude Oil
Oil density	[g/cm^3]	-	0.843 ±0.001	0.843 ±0.001	0.843 ±0.001	0.843 ±0.001	0.843 ±0.001
Oil viscosity	[mPa.s]	-	1.01 ±0.05	1.01 ±0.05	0.94 ±0.05	0.94 ±0.05	0.94 ±0.05
Slug density	[g/cm^3]	-	-	0.9751 ±0.001	0.9786 ±0.001	0.9751 ±0.001	0.9786 ±0.001
Slug viscosity	[mPa.s]	-	-	0.40 ±0.05	0.38 ±0.05	0.4 ±0.05	0.38 ±0.05
Drive density	[g/cm^3]	-	0.9717 ±0.001	0.9556 ±0.001	0.9717 ±0.001	0.9556 ±0.001	0.9717 ±0.001
Drive viscosity	[mPa.s]	-	0.37 ±0.05	0.40 ±0.05	0.37 ±0.05	0.40 ±0.05	0.37 ±0.05

*The densities and viscosities are measured at 90 ±1°C. For all experiments, except FACF0, the oil was doped with 20 wt% 1-iododecane dopant.

3.5.5 CT image processing

The use of a medical CT scanner (Siemens SAMATOM Definition) allowed for the visualization and quantification of phase saturation distributions. The images were taken using single and dual energies. The single energy 140 KeV was for measurement of two-phase saturation, whereas dual energy (80 KeV and 140 KeV) for measurements of three-phase saturations. Hounsfield units describe the CT response. These responses were then put into the listed equations in table 9 to estimate porosity (ø), S_{oi}, S_{or_WF}, S_{o_CF} and S_g.

Table 7: Formulas to calculate porosity, two phase oil saturation, three phase oil saturation and three phase gas saturation. Equations employed to estimate saturation profiles for oil and gas. The CT response in Hounsfield units for air (CT_{air}), dry core (CT_{dry}), wet core (CT_{wet}), brine in bulk (CT_{brine}) and oil in bulk (CT_{oil}). For S_{oi}, S_{or_WF} and S_{or_slug}, the two-phse oil saturation formula is used and the associated CT response for the phase is plugged into $CT_{measured.}$ For the surfactant drive co-injection phase, to calculate S_{or_CF} and the S_g the associated three phase saturation formulas are used. The number 140 is for the response with 140 KeV and 80 for the 80 KeV (Janssen & Zitha, 2018)

Parameter	Formula
Porosity ($\emptyset$)	$\frac{CT_{wet} - CT_{dry}}{CT_{brine} - CT_{air}}$
Two-phase oil saturation (S_{or}/S_{oi_WF})	$\frac{1}{\emptyset}\left(\frac{CT_{measured} - CT_{wet}}{CT_{oil} - CT_{brine}}\right)$
Three-phase oil saturation (S_{or_CF})	$\frac{(CT_{140} - CT_{140,wet})(CT_{80,dry} - CT_{80,wet}) - (CT_{80} - CT_{80,wet})(CT_{140,dry} - CT_{140,wet})}{\emptyset_{140}(CT_{80,oil} - CT_{80,brine})(CT_{140,dry} - CT_{140,wet}) - \emptyset_{80}(CT_{140,oil} - CT_{140,brine})(CT_{80,dry} - CT_{80,wet})}$
Three-phase gas saturation (S_g)	$\frac{\emptyset_{80}(CT_{140} - CT_{140,wet})(CT_{80,oil} - CT_{80,brine}) - \emptyset_{140}(CT_{80} - CT_{80,wet})(CT_{140,oil} - CT_{140,brine})}{\emptyset_{80}(CT_{80,oil} - CT_{80,brine})(CT_{140,dry} - CT_{140,wet}) - \emptyset_{140}(CT_{140,oil} - CT_{140,brine})(CT_{80,dry} - CT_{80,wet})}$

4. Results and Discussion

4.1.1 Surfactant stability in brine

The goal of the surfactant stability test in the vicinity of the original seawater injection brine composition was to examine the possibility of generating precipitations.

Table 8: Original seawater injection composition

Original Brine Composition						
Chemical	**NaCl**	**$MgCl_2$ $6H_2O$**	**$CaCl_2$ $6H_2O$**	**Na_2SO_4**	**KCl**	**$NaHCO_3$**
[wt%]	**2.425**	**0.976**	**0.141**	**0.360**	**0.063**	**0.031**

Given the seawater injection brine composition in table 10, when the surfactant is added, two major independent effects could take place. The divalent ions could interact with the surfactant yielding precipitation of anionic surfactants. The Mg^{2+} and Ca^{2+} cations screen the negatively charged sulfonate group forming complexes, and subsequently causing precipitations. Secondly, at high pH levels, inorganic salts are insoluble. So, at pH levels higher than 8.5, Mg^{2+} and Ca^{2+} ions will come out of solution causing precipitations as $Mg(OH)_2$ and $CaCO_3$, respectively. In order to test which components are mainly responsible for the precipitations, three tests were performed per surfactant. First, the full seawater brine composition was mixed with 0.30 wt% active matter (AM) of surfactant A and 0.30 wt% AM of surfactant B. Second, seawater brine was prepared without the components with divalent ions (Mg_2+ and Ca_2+) and mixed with 0.30 wt% AM of surfactant A and 0.30 wt% AM of surfactant B. Finally, seawater brine was prepared without $NaHCO_3$ and mixed with 0.30 wt% AM of surfactant A and 0.50 wt% AM of surfactant B. At the end, for every surfactants, there were three test tubes with different compositions, table 11 displays the composition of brine used for each test and the amount of surfactant added.

Table 9: Surfactant stability test in brine.

Test	**1**	**2**	**3**	**4**	**5**	**6**
Composition	NaCl $MgCl_2 * 6H_2O$ $CaCl_2 * 2H_2O$ Na_2SO_4 KCl $NaHCO_3$	NaCl Na_2SO_4 KCl $NaHCO_3$	NaCl $MgCl_2 * 6H_2O$ $CaCl_2 * 2H_2O$ Na_2SO_4 KCl	NaCl $MgCl_2 * 6H_2O$ $CaCl_2 * 2H_2O$ Na_2SO_4 KCl $NaHCO_3$	NaCl Na_2SO_4 KCl $NaHCO_3$	NaCl $MgCl_2 * 6H_2O$ $CaCl_2 * 2H_2O$ Na_2SO_4 KCl
Surfactant (A) [wt% AM]	0.30	0.30	0.30			
Surfactant (B) [wt% AM]				0.30	0.30	0.30
Precipitation	Yes	No	Yes	Yes	No	Yes

The tubes were placed in an oven under a temperature of 90 ±1ºC. Figure 6, shows the test tubes for the stability tests performed on surfactant A after 48 hours. Precipitations were seen in tube (1) and tube (3). Tube (1) was prepared with the original seawater composition. Whereas tube (3) was prepared with the seawater composition without $NaHCO_3$. In both cases precipitations were observed. However, in tube (2), where components with divalent ions (Mg_2+ and Ca_2+) are removed, no precipitations were seen. Going back to the initially explained two independent interactions that could lead to precipitation, after these tests, the most probable interaction taking place is the first one. That is the Mg_2^+ and Ca^{2+} cations interact with the charged sulfonate group forming complexes that lead to precipitations. The pH level of the different solutions prepared in the test was measured immediately after preparing the solutions. The resulting values were below 7.5, eliminating the pH level as a cause for the precipitation.

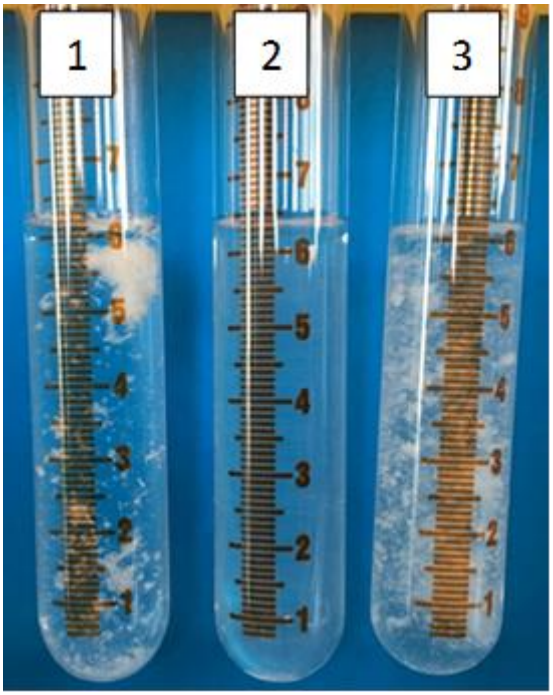

Figure 6: Surfactant A stability test. Tube 1: Original seawater composition with 0.30% AM surfactant A, Tube 2: Seawater composition without components with divalent ions (Mg_2+ and Ca_2+) and with 0.30% AM surfactant A, Tube 3: Seawater composition without $NaHCO_3$ and with 0.30 wt% AM surfactant A

4.1.2 Bulk foam

Bulk foam experiments in absence of oil were conducted to assess the capability of both surfactants to generate stable and strong foam. In bulk foam tests, as mentioned in 3.5.3, the surfactants solutions, consisting of surfactant dissolved in model brine, were placed in cylindrical tube with nitrogen gas (N_2) flowing through the solution from the bottom. Once foam column reached a fixed volume, the gas injection was shut off and foam stability was monitored as function of time. The time it takes foam to reach half of the initial foam volume is referred to as foam half-decay time. It was apparent that surfactant B was capable of generating more stable foam with a half decay time of approximately 12 hours compared with less than one hour for surfactant B, in absence of crude oil, as shown in figure 7. The quantification of half-decay time provides information about the stability of foam; the higher half-decay time, the more stable the foam is. Comparing the performance of surfactant B in absence of crude oil with other surfactants as Petrostep SB (cocoamido propyl hydroxysultaine), AOS (C_{14-16} alpha olefin sulfonate), Enorde (C_{12-15} alcohol-7EO-sulfonate) and Dowfax 8390 (alkyldiphenyloxide dsulfonate), it is ranked the highest in terms of foam half-decay time in absence of crude oil (Simjoo, 2012). Consequently, surfactant B was chosen as the foaming agent. An additional test was carried out to evaluate whether surfactant B is able to generate stable foam in presence of crude oil. The presence of crude oil is very

detrimental to the generation of foam as well as the stability of foam. In absence of oil, foam generated by surfactant B solution had a half-decay time of approximately 12 hours, however, in the presence of crude oil, the half-decay time dropped to nearly 1.43 hours, figure 7. In comparison with the previously mentioned surfactants, AOS ($C_{14\text{-}16}$ alpha olefin sulfonate) exhibits relatively the same foam half-decay time as surfactant B solution in presence of crude oil. A drop of foam half decay time of a factor of eight due to the presence of oil illustrate how large of an impact crude oil can make to the generated foam. This was examined further in the results yielded by the foam generation experiment at S_{or_WF}.

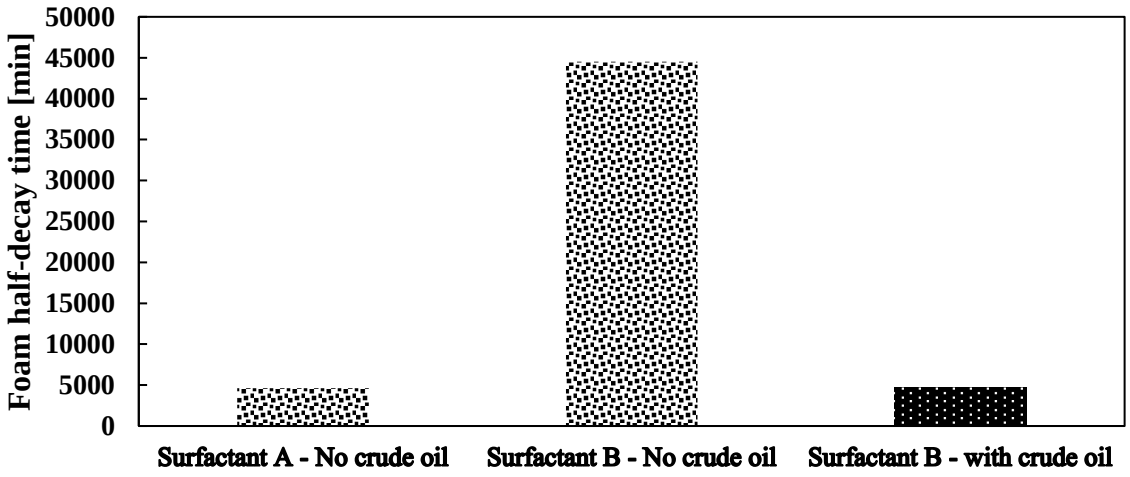

Figure 7: Bulk foam test for surfactant A and B in absence of crude oil, and for surfactant B in presence of crude oil.

Table 10: Surfactant B drive solution composition used in bulk foam analysis. For the surfactant, 0.5wt% of AM was used

Drive foam solution composition	
Additive	Weight %
NaCl	3.353
$MgCl_2$ 6 H_2O	0.000
$CaCl_2$ $2H_2O$	0.000
Na_2SO_4	0.360
KCL	0.063
$NaHCO_3$	0.031
Surfactant B	0.50*

4.1.3 Phase behaviour

The aim of the phase behaviour study is to determine the surfactant agent to be used as an o/w IFT lowering agent. By the end of this test, a surfactant slug formulation was chosen with the proper salinity range to mobilize S_{or_WF} by lowering the o/w IFT. The salinity of the system is a key factor for any given surfactant to lower the o/w IFT (Janssen, et al., 2018). By varying the concentrations of NaCl and KCl, a big range of salinities was achieved to determine where the optimum salinity conditions are. Having two surfactants to choose from, both of them underwent the same test. The surfactant concentration was kept constant at 0.30 AM wt% for surfactant A, and 0.30 AM wt% for surfactant B. The other components were kept constant, consisting of crude oil at 1:2 oil-to-water ratio, 1.00 wt% sec-butanol, 0.37 wt% Na_2SO_4, and 0.32 wt% $NaHCO_3$. Figure 8 shows the 14 salinities studied corresponding to surfactant A., and figure 9 shows the second test with surfactant B after reaching equilibrium. In both tests, a micro-emulsion was present between oil and water phases in the salinity ranges between 0 and 0.40 wt%. The presence of this micro-emulsion at very low salinity ranges is most probably due to the natural surfactants present in the crude oil. In fact, when crude oil was tested with demineralized water, a small layer of micro-emulsion was formed after 24 hours, as shown in figure 10. Figure 8 shows distinct micro-emulsion observed in the tubes with 1.50 wt% and 1.75 wt% NaCl+KCl for the salinity test with surfactant A. For the salinity test with surfactant B, no visible micro-emulsion layer was observed in all of the salinity ranges.

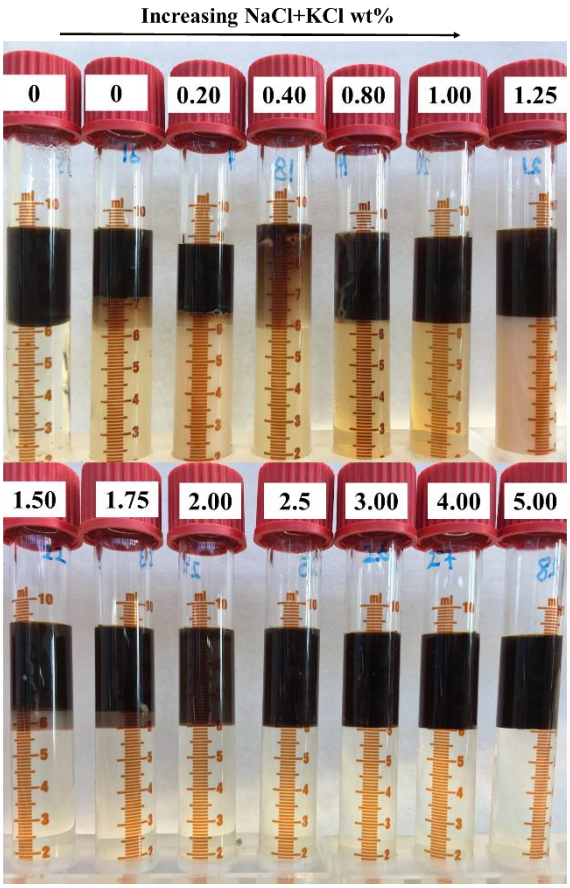

Figure 8: Salinity scan performed with different combinations of NaCl+KCl concentrations for surfactant A. The fist tube on the top left side was prepared without NaCl+KCl and without surfactant, whereas the tube next to it was prepared without NaCl+KCl

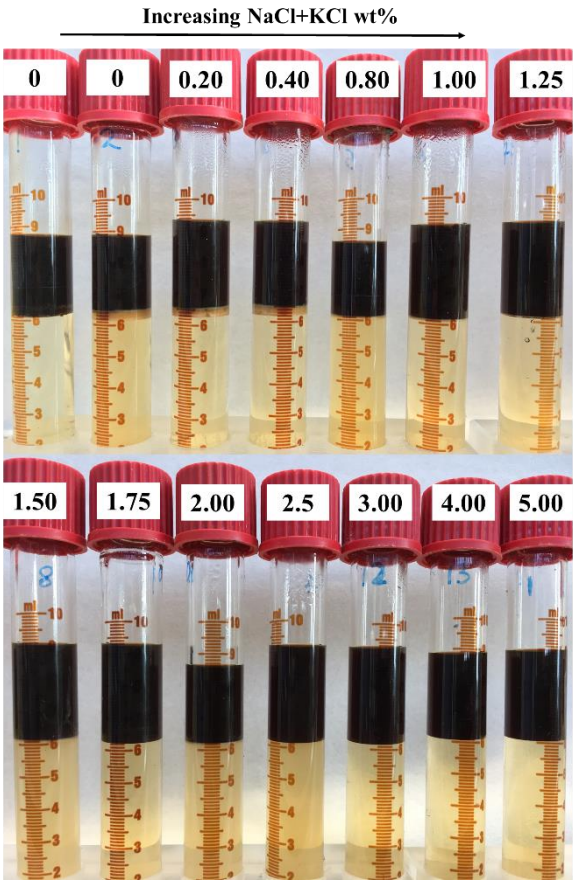

Figure 9: Salinity scan performed with different combinations of NaCl+KCl concentrations for surfactant B. The fist tube on the top left side was prepared without NaCl+KCl and without surfactant, whereas the tube next to it was prepared without NaCl+KCl

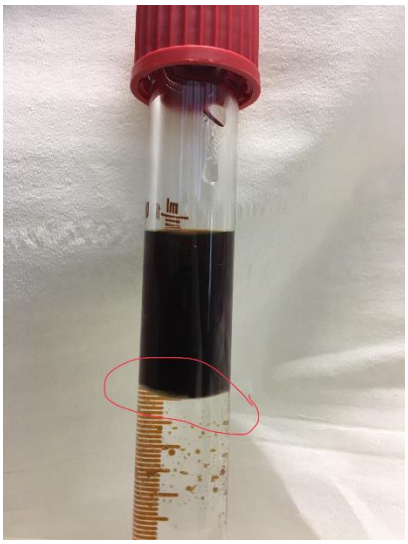

Figure 10: Crude oil and demineralized water test. The circled area shows a small micro-emulsion layer observed after 24 hours

Since a distinct micro-emulsion was only observed in the salinity scan performed with surfactant A, as shown in figure 8, the amount of oil and water that went into micro-emulsion

were measured. Then, the solubilisation parameters (SP) were estimated by applying the following formulas:

$$SP_O = \frac{V_O}{V_S} \; ; \; SP_W = \frac{V_W}{V_S} \qquad \textit{Equation 4}$$

where V_o is the volume of oil solubilised in emulsion phase, V_w is the volume of water solubilised in emulsion phase and V_s is the volume of surfactant solubilized in the emulsion phase (Sheng, 2013). Afterwards, by using Huh's empirical formula, the oil/micro-emulsion and water/micro-emulsion IFT values were estimated as follows:

$$\sigma_{mo} = \frac{C_{Ho}}{SP_O^2} \; ; \; \sigma_{mw} = \frac{C_{Hw}}{SP_w^2} \qquad \textit{Equation 5}$$

where σ_{mo} is the oil/micro-emulsion IFT, σ_{mw} is the water/micro-emulsion IFT, C_{Hw} and C_{Ho} are emperical constants that range between 0.1 to 0.35, typically 0.3 is used for experimental data (Sheng, 2013) . The water and oil solubilisation ratios, as well as water/micro-emulsion and oil/micro-emulsion were plotted as functions of salinity [NaCl+KCl wt%], figure 11. The intersection point corresponds to Winsor Type (III) with the lowest o/w IFT. As showen in figure 11, the point of optimum salinity is 1.5 NaCl+KCl wt%. In addition, the lower phase range is from 0 to 1.25 NaCl+KCl wt%, middle phase from 1.3 to 1.75 NaCl+KCl wt% and the upper phase is above 1.75 NaCl+KCl wt% (Sheng, 2013).

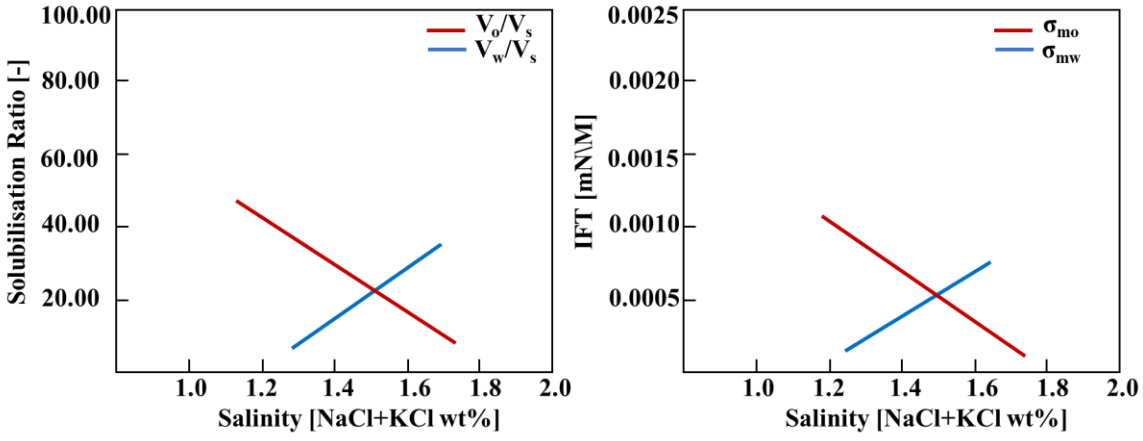

Figure 11: On the left, the solubilisation ratio is represented as a function of salinity [NaCl+KCl] for salinity test prepared with surfactant A. On the right, the corresponding water/micro-emulsion and oil/micro-emulsion IFT as a function of salinity [NaCl+KCL wt%].

From these tests and observations, surfactant A was chosen as o/w IFT reduction agent to be used in the formulation of surfactant slug solution. For surfactant B, it was impossible to carry out the same performed calculation, given that no distinct micro-emulsion phase was observed.

Since two FACF experiments are planned to be performed with medical CT-scan assistant, 20 wt% of 1-iododecane will be added to the crude oil (oleic phase). To evaluate the effect of dopant addition to the optimum salinity condition, an additional salinity test was carried out. In this test, the concentrations of NaCl and KCl were varied from 0.5 to 4 NaCl+KCL wt%. Surfactant A concentration was kept constant at 0.30 AM wt%. The other components were kept constant, consisting of crude oil with 20 wt% 1-iododecane at 1:2 oil-to-water ratio, 1.00 wt% sec-butanol, 0.37 wt% Na_2SO_4, and 0.32 wt% $NaHCO_3$. Figure 12 shows the 9 salinities studied corresponding to surfactant A, where 20 wt% of 1-iododecane was added to the crude oil. In the same figure, distinct micro-emulsion was observed in the tubes with 1.50 wt% and 1.75 wt% NaCl+KCl, the same as in the case without 1-iododecane.

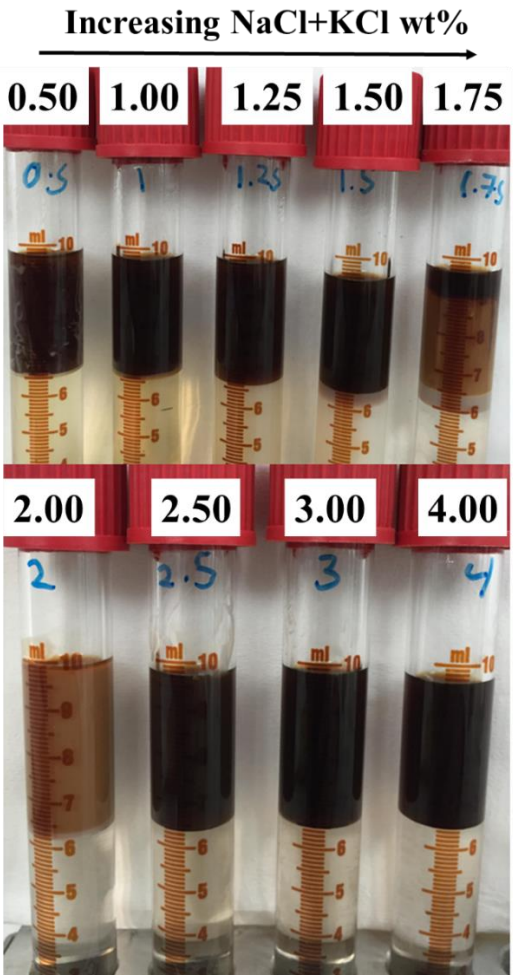

Figure 12: Salinity scan performed with different combinations of NaCl+KCl concentrations for surfactant A, where 20 wt% 1-iododecane were added to the crude oil.

The SP_o and SP_w were calculated again, as well as the σ_{mo} and $\sigma_{mw,}$ and plotted as functions of salintity, figure 13. From figure 13, the intersection point is the same as in the case where no dopant was added. However, there is a change in the solubilisatioin ratio. In this case, the solubilisaton ratio is higher than the case where no dopant was added, resulting in a slightly lower water/micro-emulsion and oil/micro-emulstion IFT's.

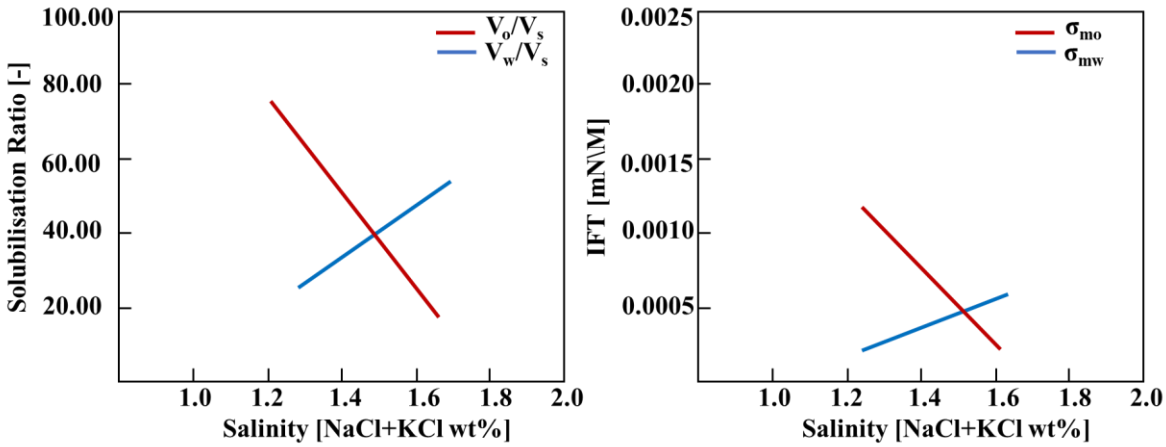

Figure 13:Solubilisation ratio and IFT plots. On the left, the solubilisation ratio is represented as a function of salinity [NaCl+KCl] for salinity test prepared with surfactant A and crude oil with dopant. On the right, the corresponding water/micro-emulsion and oil/micro-emulsion IFT as a function salinity [NaCl+KCL wt%]

The salinity scan of slug surfactant A solution with crude oil in presence of 20 wt% 1-iododecane and in its absence, yielded the same point of optimum salinity at 1.5 NaCl+KCl wt% (figure 11 and 13). In addition, the lower phase range is at from 0 to 1.25 NaCl+KCl wt%, middle phase from 1.3 to 1.75 NaCl+KCl wt% and the upper phase starts above 1.75 NaCl+KCl wt% (Sheng, 2013).

In the FACF experiments, the effect of salinity on the slug surfactant solution is to be evaluated. Therefore, two experiments were desiged with under-optimum salinity surfactant slug solution, and another two with optimum salinity surfactant slug solution. Subsequently, the salininties associated with these two were 1.00 NaCl+KCl wt% for under-optimum and 1.75 NaCl+KCl wt% for optimum salinity conditons were chosen for the formulation of the slug solution. Table 13 shows the final surfactant slug A composition for both under-optimum and optimum salininty conditions.

Table 11:Final Surfactant slug composition

Surfactant slug solution composition		
Salinity condition	**Under-optimum salinity**	**Optimum salinity**
Additive	Weight %	Weight %
NaCl+KCl	1.000	1.750
$MgCl_2$ 6 H_2O	-	-
$CaCl_2$ $2H_2O$	-	-
Na_2SO_4	0.369	0.369
$NaHCO_3$	0.032	0.032
Sec-butanol	1.000	1.000
Surfactant A	0.30 AM	0.30 AM

4.1.4 Foam generation in absence and presence of oil in sandstone

Core-flood 1 (table 6) was performed to assess the possibility of generating strong and stable foam using final surfactant B drive solution (table 13), in porous media and in absence of crude oil under reservoir conditions (at 90 ±1ºC and 20 bar back pressure). Foam apparent viscosity were calculated by rearranging Darcy's equation (Falls, et al., 1980).

$$\mu_{apparent} = \frac{k}{Q}\frac{\Delta P\ A}{L} \qquad \textit{Equation 6}$$

where k is the absolute permeability in m^2, Q is the flow rate in m^3/sec, ΔP is pressure drop across core cross-sectional area in Pa, A is the area in m^2 and L is the length of the core. Figure 14 shows that the critical gas fraction (fg), i.e. critical foam quality, equals 75 %, after which the foam apparent viscosity starts to decrease with increasing gas fraction yielding unstable foam.

The second core-flood experiment (core-flood 2, table 6) took place afterwards to investigate the possibility of generating foam at S_{or_WF}. A previous experimental study that utilized multiple drive foam qualities showed that lower drive foam qualities favour oil bank displacement and yield more stable foam in the presence of oil (Janssen, et al., 2018). It was for this reason that a foam quality of 57.5% was used in core-flood 2. Co-injection was initiated right after the water flooding process. Figure 8 shows the total pressure drop as a function of PV injected.

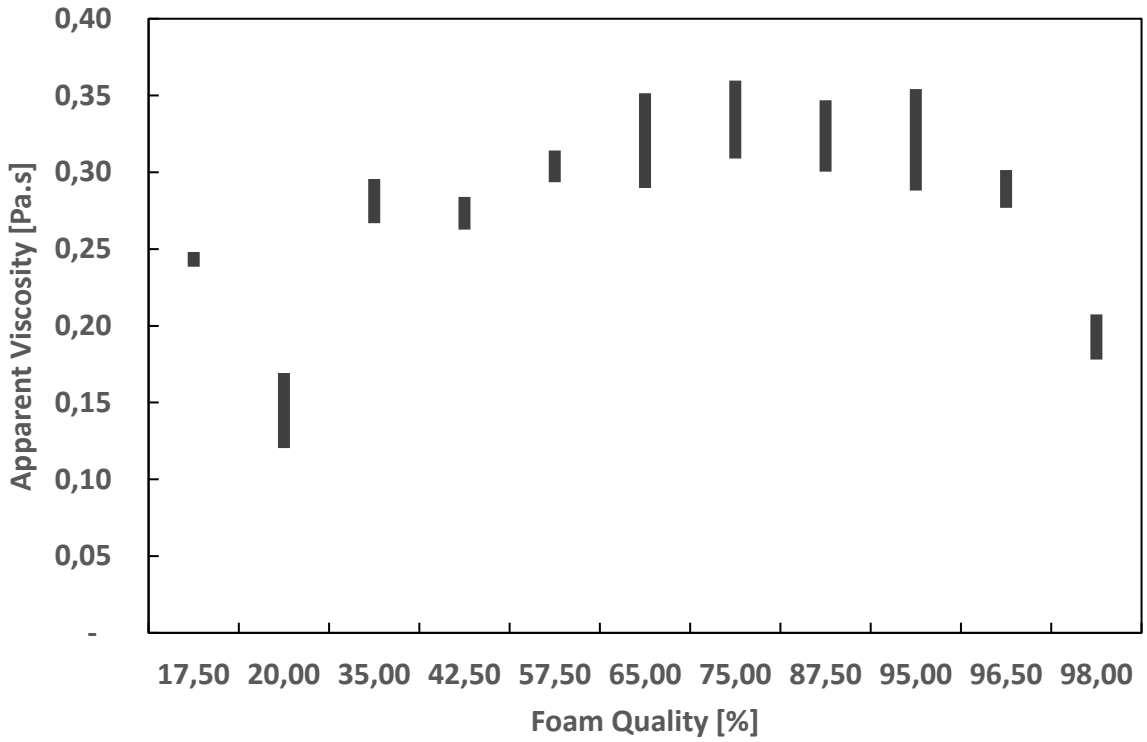

Figure 14: Foam apparent viscosity as function of foam quality obtained during core-flood 1.. The black bars represent the highest and lowest achieved apparent viscosity per foam quality.

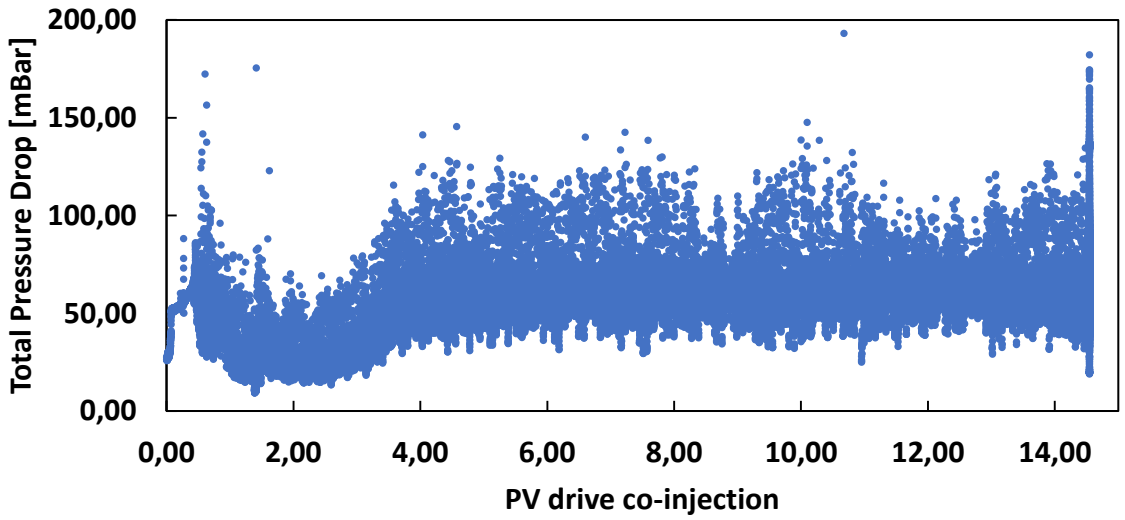

Figure 15: Total pressure drop as function of PV drive co-injection. Zero total PV corresponds to the beginning of co-injection

The total pressure drop graph along with both visual evaluation of effluents and an observed gas breakthrough time of 0.37 total PV injected, suggests that no foam was generated during this experiment. A question to be asked is why foam was not generated. In the study of Simjoo (2013) it was possible to generate foam at S_{or_wf} . However, in that study, the oil utilized was a synthetic Hexadecane oil. In this experiment, crude oil was utilized. Simjoo (2013) studied the effect of different oils (n-C_6, n-C_{10} and n-C_{16}) on the rate of bubble coalescence. It was shown that as the chain length of the alkane decreases, the coalescence rate becomes higher, and subsequently the half-decay time of foam becomes smaller. The crude oil that has been utilized in this experimental study consists of 14 wt% C_8, 50 wt% C_6-C_{12} and 80 wt% C_6-C_{18}. As the crude oil composition is relatively dominated by short chains, its impact on reducing foam stability becomes higher. The literature shows that crude oil has a complex interaction with foam, and the complexity is increased in a dynamic system rather than a static system. In fact, some has suggested that there is an oil saturation above which foam cannot be formed (Schramm, 1994). Hence, the presence of high concentration of oil could be another reason for not generating foam. Going back to section 4.1.2 (bulk foam analysis), it provides a strong evidence that crude oil is very detrimental to the generation of foam and its associated stability. However, does this imply that it is not possible to generate stable drive foam in the upcoming full EOR core-flood experiments? A crucial point here is that in the full FACF core-flood experiments a surfactant A slug (table 13) will be injected subsequent to waterflooding; most likely reducing S_o near the inlet section. This might provide space near the inlet, exhibiting relatively low S_o, for stable foam to be generated during drive co-injection prior to reaching to the oil bank (high S_o).

4.1.5 FACF core-flood experiments

In this section, the four performed FACF experimental results are presented (table 8). Table 14 showcases the main results of the four experiments. Both CT data and material balance data are presented and they are in good agreement. This chapter is divided into different sections to shed some light on the effect of slug salinity and pre-generated foam on the FACF efficiency. This chapter is divided into the various injection stages. It includes primary drainage and forced imbibition, surfactant A slug injection for the mobilization of residual oil, and displacement of mobilized oil by foam through the co-injection of surfactant B drive solution with N_2.

Table 12: Summary of full EOR FACF results. kro is the end point relative permeability of oil, and krw* is the end point relative permeability of water. MB represents the material balance equation results, whereas CT represents the results estimated from CT-scan response. S_{wc} is the connate water saturation, S_{oi}, is the initial oil saturation, S_{or_wf} is the residual oil to waterflood, and S_{or_cf} is the residual oil after co-injection.. R_{FWF} is the recovery factor achieved after waterflooding, and R_{FCF} is the recovery factor achieved after co-injection.*

Parameter	**FACF0**	**FACF1**		**FACF2**		**FACF3**
$\mathbf{k_{ro*}}$	0.47 ±0.04	0.54 ±0.06		0.60 ±0.06		0.65 ±0.04
$\mathbf{k_{rw*}}$	0.18 ±0.05	0.21 ±0.05		0.24 ±0.07		0.19 ±0.05
Parameter	**FACF0**	**FACF1**		**FACF2**		**FACF3**
	MB	**MB**	**CT**	**MB**	**CT**	**MB**
$\mathbf{S_{wc}}$	0.21 ±0.02	0.25 ±0.02	0.20 ±0.01	0.26 ±0.02	0.21 ±0.01	0.20 ±0.02
$\mathbf{S_{oi}}$	0.79 ±0.02	0.75 ±0.02	0.80 ±0.08	0.74 ±0.02	0.84 ±0.08	0.80 ±0.02
$\mathbf{S_{or\_WF}}$	0.36 ±0.01	0.29 ±0.01	0.31 ±0.01	0.31 ±0.02	0.33 ±0.02	0.34 ±0.02
$\mathbf{R_{FWF(\%of\ OIIP)}}$	55.00 ±3.00	61.00 ±3	61.00 ±9	59.00 ±3	61.00 ±10	46.00 ±3
$\mathbf{S_{or\_CF}}$	0.23 ±0.01	0.17 ±0.01	0.20 ±0.06	0.20 ±0.01	0.21 ±0.03	0.16 ±0.01
$\mathbf{R_{FCF(\%of\ OIIP)}}$	70.00 ±5	77.00 ±5	75.00 ±14	73.00 ±5	75.00 ±11	80.00 ±5

4.1.5.1 Primary drainage and forced imbibition

In all of the FACF core-flood experiments, the two preliminary steps performed were primary drainage and forced imbibition. In primary drainage, oil is being injected into the core to establish S_{wc}. Afterwards, waterflooding was initiated to establish S_{or_WF}. Total pressure drop profiles, CT images and associated saturation profiles are presented and discussed in this section. Note that only experiments FACF1 and FACF2 were performed with the assistance of a medical CT scanner.

Pressure drops

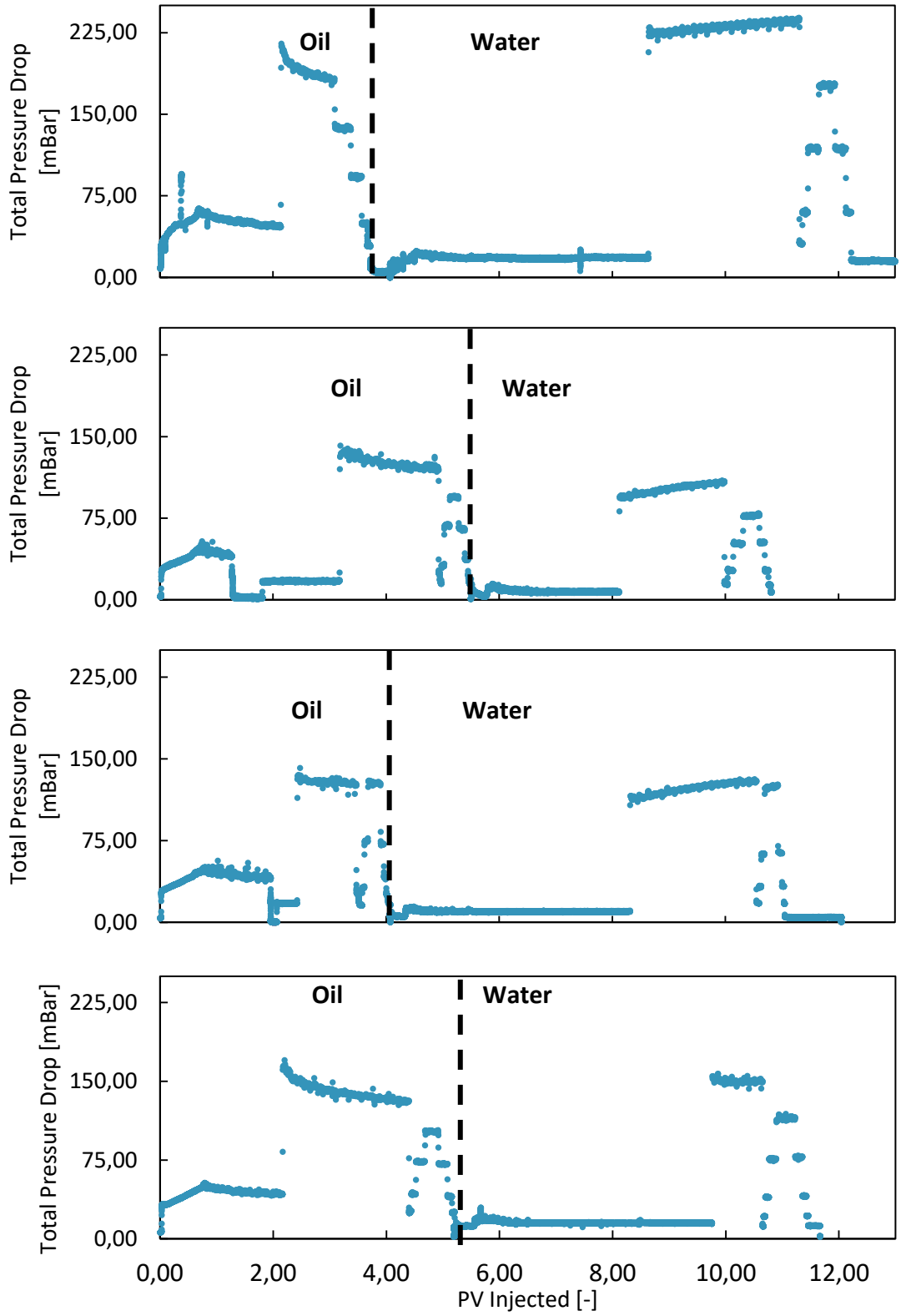

Figure 16: Total pressure drop during primary drainage and forced imbibition. In FACF0, Oil injection started at 0.5 cm3/min and was stopped at two occasions in the beginning for a suspected leak in the system. After confirming no leak was present, the injection was continued at 0.5 cm3/min. Bump flooding was initiated with 4 cm3/min, then end point relative permeability estimation process started by lowering the rate to 3, 2, 1 and 0.5 cm3/min. At the end, the rate was reduced to 0.05 for overnight. In FACF1, oil injection started at 0.5 cm3/min then it was reduced to 0.1 cm3/min after 1.7 PV for overnight, then injection was resumed at 0.5 cm3/min. For end point relative permeability rate was varied from 0.5 to 1, 2, and 3 cm3/min. in FACF2, oil injection started at 0.5 cm3/min, then was reduced for overnight to 0.0125 cm3/min after 2 PV

and later it was increased to 0.5 cm3/min. For end point permeabilities the rate was varied from 0.5 to 1 and 2 cm3/min. In FACF3, oil injection started at 0.5 cm3/min, then bump flooding was performed by increasing the rate to 4 cm3/min, followed by end point relative permeability estimation by varying the rate from 0.5 to 1, 2 and 3 cm3/min. For the forced imbibition, in all cases, waterflooding started at 0.25 cm3/min, then after no oil production was observed, bump flood was initiated by increasing flow to 4 cm3/min. End point relative permeability estimation was performed by varying the rate from 0.25 to 0.5, 1, 2 and 3 cm3/min.

Figure 16 presents the total pressure drop profiles for the four FACF experiments performed during primary drainage (i.e. oil injection) and forced imbibition (i.e. water flooding). During primary drainage, an instant increase in pressure drop is observed as the oil gets in contact with the core, indicating capillary pressure, reaching an approximate value of 40 ±3 mBar. As the oil propagates through the core, the pressure drop continues to increase gradually until oil breaks through at 0.75±0.01 PV for FACF0, 0.72±0.01 PV for FACF1, 0.80±0.01 PV for FACF2, while it breaks though at 0.76±0.01 PV for FACF3. Afterwards the total pressure drop in FACF0 decreases gently to reach steady state pressure at approximately 47±3 mBar after 1.80±0.01 PV of crude oil injected. For FACF1, FACF2 and FACF3 slight decrease follows oil breakthrough, then pressure drop remains constant at 43±3 mBar for FACF1, 41±3 mBar for FACF2 and 43±3 mBar for FACF3 with oil injection rate of 0.5 cm^3/min. Bump flood is then performed to ensure that all movable water is produced to reach S_{wc} conditions. This can be seen in the sharp decrease in total pressure drop after the initial spike followed by a stabilization period. For FACF0, the spike in pressure drop is observed after 2.14±0.01 PV of oil injected reaching to approximately 225±3 mBar. For FACF1 the spike in total pressure drop is at 3.17±0.01 PV and recording a total pressure drop of 150±3 mBar. In FACF2 total pressure drop reached 147±3 mBar at 2.42 ±0.01 PV. For FACF3, the total pressure drop spike is seen after 2.16 ±0.01 PV and reaching a value of 160±3 mBar. In FACF0, the total pressure drop is relatively higher during the bump flooding stage, this could be due to the relatively lower absolute permeability value of the core compared to the rest of the FACF core samples (table 4). The area where the total pressure drop has reached to steady state can be identified in FACF1, FACF2 and FACF3. However, it is not clearly identifiable in FACF0. This could be attributed to the fact that true S_{wc} was not reached and mobilized water was still being produced. For water flooding, relatively lower total pressure drops were achieved due to the use of lower flow rates, and the associated relatively low viscosity of the fluid being injected. Water breakthrough took place at approximately 0.38 ±0.01 (FACF0), 0.31 ±0.01 (FACF1), 0.35 ±0.01 (FACF2) and 0.39 ±0.01 (FACF4) PV of water injected. The total pressure drop follows the same trend in all of the experiment, except for FACF0, as it shows relatively higher drop, same as in the primary drainage process. That is due to the low absolute permeability value

(table 4). Bump flooding is performed again to reach S_{or_WF} conditions. As shown in the graphs, in experiments FACF0, FACF1 and FACF2, the total pressure drop keeps increasing gently during the bump flood process and does not reach steady state conditions. That implies that in these scenarios, some amount of oil was still being mobilized and maybe produced. By analysing a simplified one dimensional Darcy equation for fractional flow, it can be easily explained.

$$\Delta P = u_{total}\left(\frac{\mu_o}{k_{ro}k} + \frac{\mu_w}{k_{rw}k}\right)L \qquad \textit{Equation 7}$$

where μ is the viscosity of oil and water, k is the absolute permeability, k_r is the relative permeability of the phase, u_{total} is the superficial velocity and L is the length of the core. If only water flows, then the oil terms are eliminated, leaving only the water terms. This may lead to lower pressure drop values. However, it depends on the magnitude of the effect of each phase. Apparently, the increase in water relative permeability has a bigger effect on pressure drop than the decrease in oil relative permeability. Most likely, the increase in water mobility outweighs the reduction of oil mobility to zero in terms of overall pressure drop, which yields higher pressure drops for single phase water flow at S_{or_WF} compared to two-phase flow at the same superficial velocity. On the other hand, the total pressure drop shown in FACF3 during the bump flood stage, shows an initial spike followed a plateau, indicating that residual conditions were met. After the bump flood, flow rates were varied to estimate the end-point relative permeability values k_{ro*} and k_{rw*}.

CT images and oil saturation profiles

In this section, the CT images (A) along with the saturation profiles (B) captured during the primary drainage and forced imbibition stages for both FACF1 and FACF2 are presented and discussed. In both experiments, a slight change to the experimental setup was done. To impose reservoir conditions throughout the experiments, a temperature of 90±1^{o}C must be maintained. In order to satisfy this condition while performing the experiment with CT assistance, metal sleeves were placed around the core-holder, and connected to a liquid heating machine, figure 17. The liquid is heated to the desired temperature and circulated through the metal sleeves to maintain the required temperature. Four sleeves were utilized to cover the core-holder; two from bottom and two from top. However, a small gap was present between the sleeves. This gap resulted in scattered CT responses that do not correspond with the rest of CT responses for areas covered by the heating metal sleeves. In all of the processed CT images, the response of the area falling within the gap was not neglected.

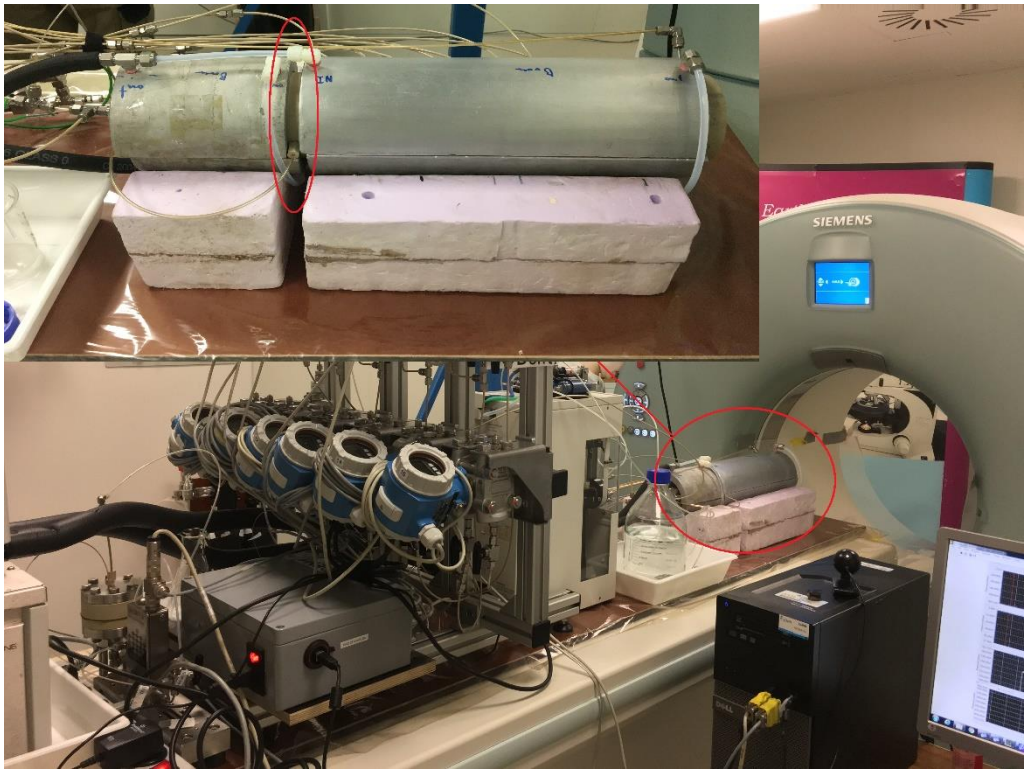

Figure 17: FACF1 and FACF2 modified setup for CT-scanner. The zoomed-in image shows the metal sleeves covering the core-holder. the circled area in the zoomed-in picture represents the gap between the sleeves.

Figure 18 and 19, show the processed CT images and saturation profiles for primary drainage and forced imbibition stages for FACF1 and FACF2. In both experiments (FACF1 and FACF2), during primary drainage (figure 18A and 19A), it can be seen that brine (blue) was displaced by oil (red). The capillary end effect is seen in both cases at the end of the cores where large water accumulation is achieved during primary drainage (red indicates oil and blue indicates water). Water, as a wetting phase, accumulates at the outlet section to satisfy the zero capillary pressure condition. During primary drainage, a Buckley-Leverett displacement can be seen. On the other hand, during waterflooding, a less sharp front is seen as a result of capillary forces. It can be seen that the injected water was not displacing the oil in a favourable, frontal manner. In fact, in both experiments, water seems to be fingering through the oil bearing part of the reservoir, resulting in an unstable front.

Oil saturation profiles during primary drainage and waterflooding for core-flood FACF1 and FACF2 are presented respectively in figures 18B and 19B. Note the relatively low S_o near the outlet region at the end of primary drainage in both experiments as a result of the capillary end effect. The end-point mobility ratios can be calculated using the following formula:

$$M = \frac{\frac{k_{rw}}{\mu_w}}{\frac{k_{ro}}{\mu_o}}$$ *Equation 8*

where k_{rw} and k_{ro} are the endpoint relative permeability of water and oil, respectively. The mobility ratios are equal to 1.01±0.02 for FACF1 and 1.05±0.03 for FACF2. For favourable mobility conditions, the mobility ratio should be lower than one (Pal, et al., 2017).

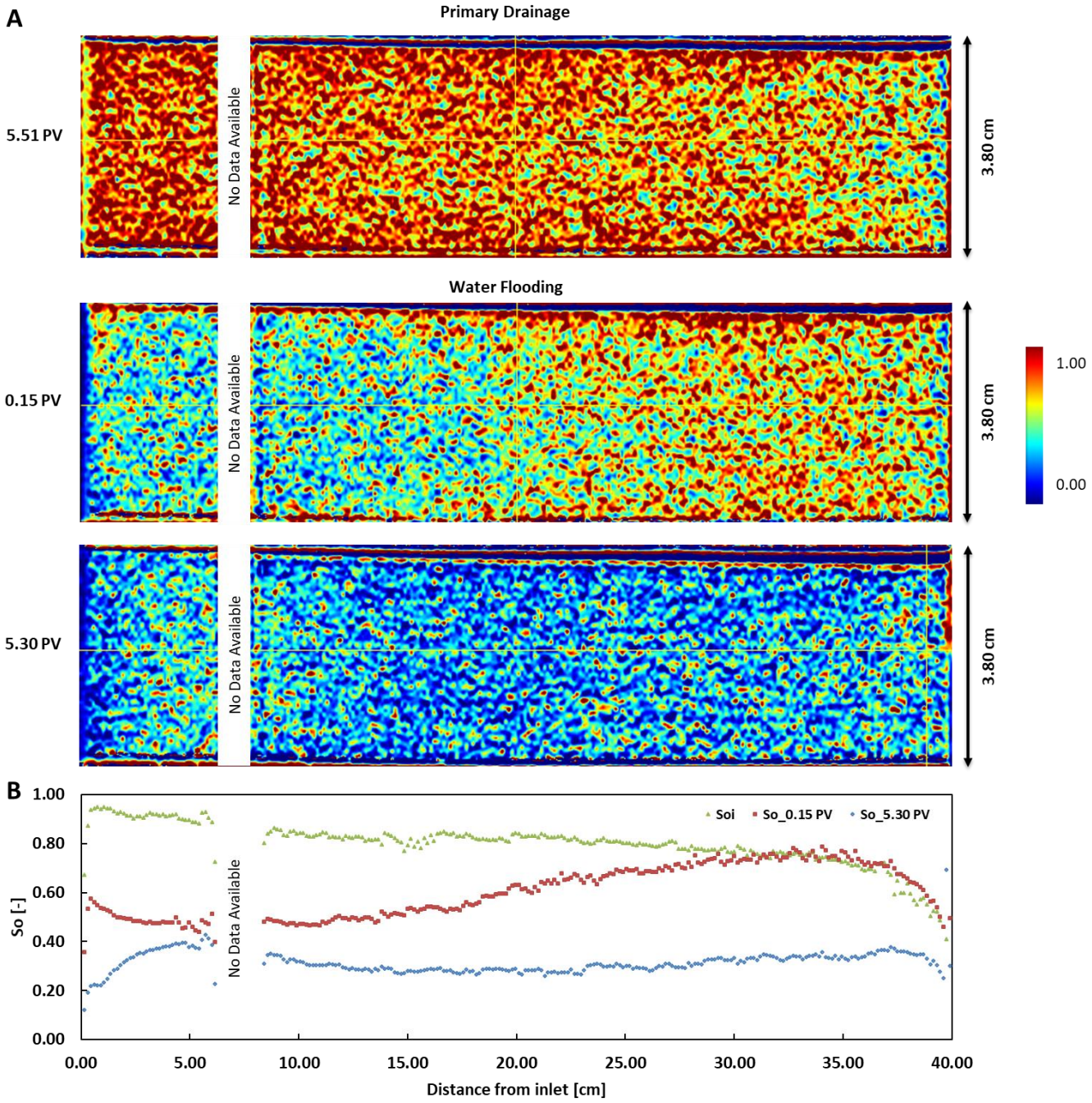

Figure 18: FACF1 - CT images (A) and oil saturation profiles (B) for the primary drainage and forced imbibition injection stages in FACF2. Brine is shown in blue and oil in red

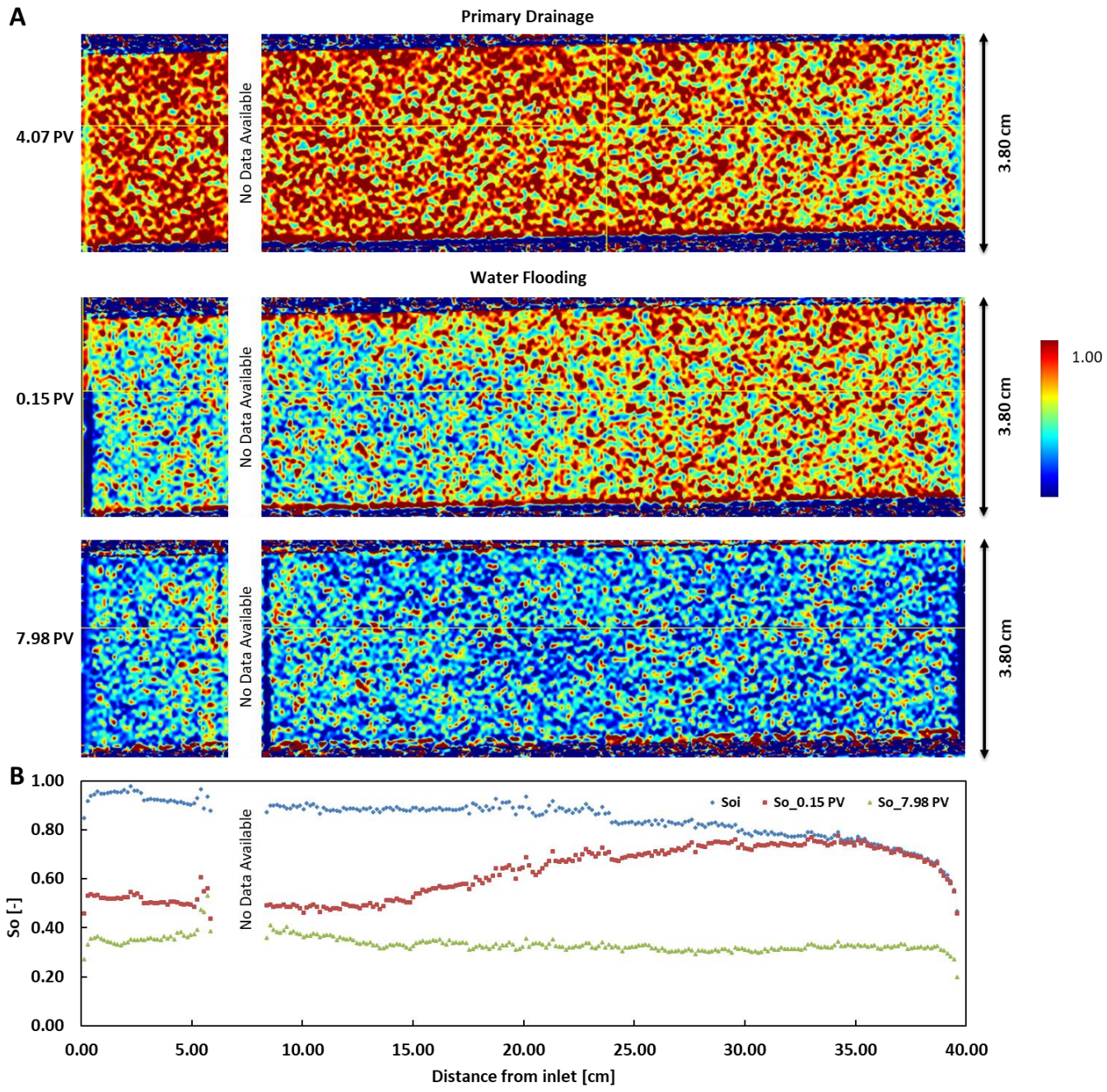

Figure 19: FAFC2 - CT images (A) and oil saturation profiles (B) for the primary drainage and forced imbibition injection stages in FACF2. Brine is shown in blue and oil in red

4.1.5.2 Mobilization of residual oil

In this section, the results of injecting surfactant slug (table 13) in order to mobilize S_{or_WF} are presented. Total pressure drop data, CT images and corresponding saturation profiles are listed

to complement each other and help draw a qualitative and quantitative understanding of the formation of oil bank.

Pressure drops

Figure 20 shows the total pressure drop data for the surfactant slug injection phase. The pressure drop remained steady throughout the entire injection process. Pressure drop is highly affected by viscosity and relative permeability. In general, pressure drop profiles during surfactant slug injection can follow different trends depending on the fluid mobilities and saturation distributions.

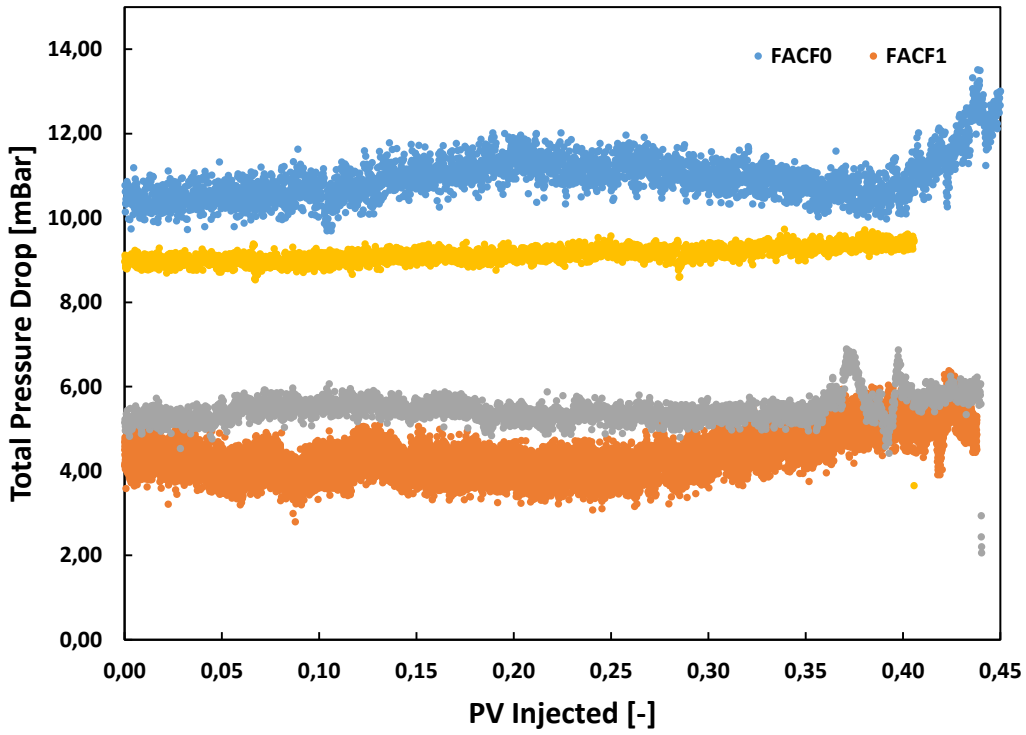

Figure 20: Total pressure drop for FACF experiments during the surfactant slug injection process

CT images and saturation profiles

Figure 22 and figure 23 present the processed CT images and saturation profiles associated with the surfactant slug injection phase. The CT images along with the saturation profiles during surfactant slug injection process were taken at the same time (0.06, 0.23 and 0.44 PV injected). It is evident that the formed oil bank displacement in both FACF1 and FACF2 is not stable. For FACF1, no oil bank is seen at the first two CT scans. However, given that the presented CT images are in the centre of the core, by looking at a different cross-sectional view

it can be seen that oil was not accumulated in the exact centre, figure 21. As it can be seen from the CT images, the oil accumulation over time is creating a shape with a leading edge and a trailing tail in both FACF1 and 2. Peak S_o values, after 0.44±0.01 PV injected were found to be 0.44±0.02 for both FACF1 and FACF2. The average S_o upstream of the oil bank after 0.44±0.01 PV injected is 0.28±0.06 and 0.32±0.04 for FACF1 and FACF2 respectively.

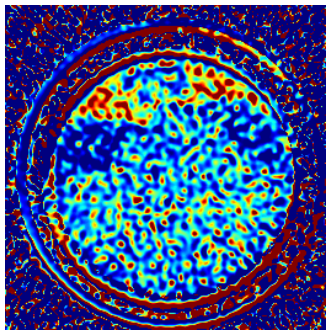

Figure 21: FACF1 CT image at a distance of 6 cm from inlet showing oil accumulation at the uppermost part of the core

In order to assess the stability of a displacement front, one may use the mobility ratio (Sheng, 2011). Why would the oil bank propagation be unstable? One approach to answer this question is by explaining the effect of mobility ratio. It is defined as the "ratio of the displacing phase mobility to the displaced phase mobility" (Sheng, 2011).

$$M = \frac{\lambda_{upstream}}{\lambda_{downstream}} \qquad \textit{Equation 9}$$

In this equation, M is the mobility ratio, and λ is the mobility for upstream and downstream phase. For a favourable mobility, M must be less than one. Therefore, the unfavourable mobility condition could be a result of the mobility of the fluid upstream of the trailing edge and just within the oil bank being higher than that of the fluid in the downstream.

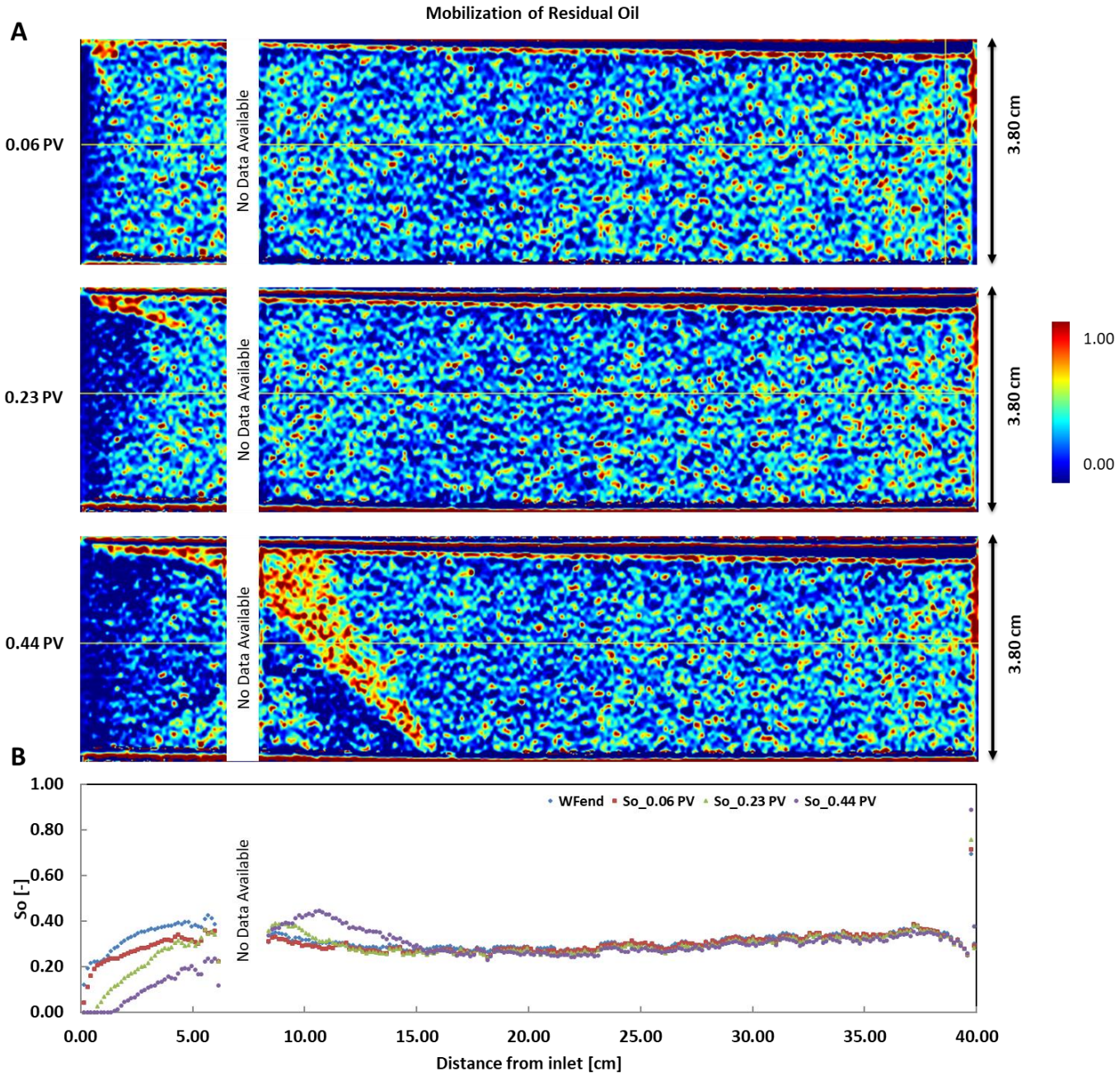

Figure 22: CT images (A) and oil saturation profiles (B) for the surfactant slug injection process in FACF1

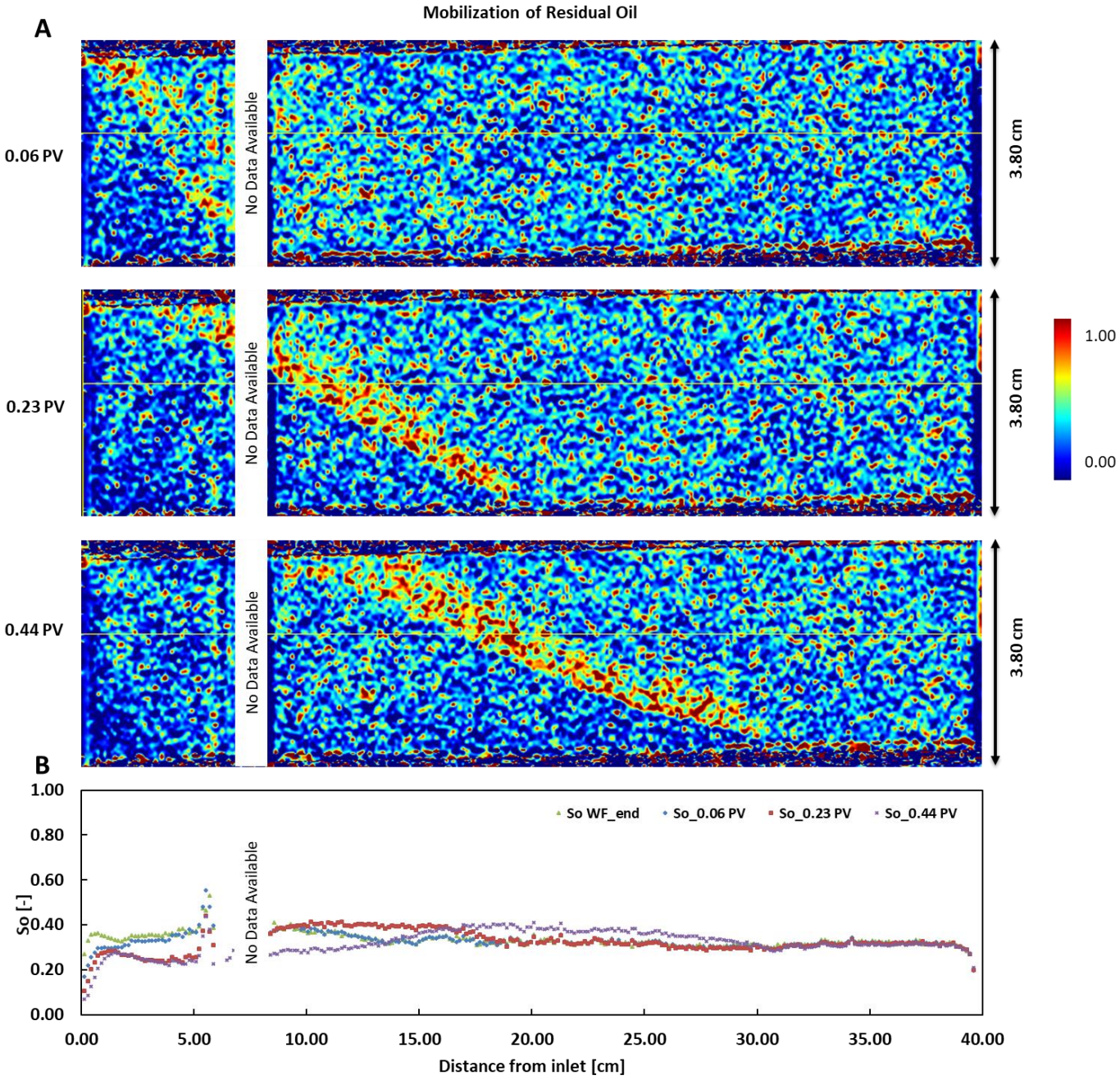

Figure 23: CT images (A) and oil saturation profiles (B) for the surfactant slug injection process in FACF2

4.1.5.3 Displacement of mobilized oil by foam

In this section the results of the co-injection of N_2 and surfactant drive solution to generate foam are presented. Total pressure drop data along with CT images and oil and gas saturation profiles are studied and analysed to assess whether foam was generated or not, and to have a clear picture of oil displacement by foam.

Pressure drops

The total pressure drop profiles presented in figure 24, show similar trends for FACF0, FACF1 and FACF2 initially. As soon as co-injection starts, an increase in total pressure drop is observed towards 30±3 mBar for the three experiments due to the entrance of the co-injected surfactant drive and gas phase into the core. After that spike in total pressure drop, FACF0 and FACF2 show a similar constant trend as foam propagates through core. A constant trend is followed, during which oil breakthrough takes place at 0.22±0.01 PV for FACF0 and 0.13±0.01 PV for FACF2. Then, total pressure drop remains stable until gas breaks through at 0.43±0.01 PV for FACF0 and 0.58±0.01 PV for FACF2. In FACF1, after the initial spike in pressure drop, a slightly gradual increase of pressure drop is seen as foam propagates through the core section. During this period, oil breakthrough takes place at 0.17±0.01 PV. The gradual increase in pressure drop continues until gas breakthrough at 0.48±0.01 PV. Afterwards, the pressure drops start descending gradually. For the last experiment FACF3, the spike in pressure drop is also seen as soon as co-injection is initiated, to reach a value of 32±3 mBar. Following this spike, the pressure drop starts increasing from 32±3 mBar gradually to reach 40±3 mBar at 0.20±0.01 PV. During this period, foam propagates throughout the first section of the core. Afterwards, a sharp increase is observed in total pressure drop to hit 55±3 mBar at 0.19±0.01 PV. This happened slightly before oil breakthrough at 0.20±0.01 PV. A constant trend in total pressure drop follows while displacing the oil bank. A gradual increase in total pressure drop is noticed from 0.35±0.01 PV until it reached a pressure drop second peak at 0.50 ±0.01 PV, as foam is propagating from section to section along with the displaced oil through the core. With all of the displaced oil reaching the outlet section and exiting the core, the total pressure drop starts descending. It continues decreasing until gas breaks though at 0.80 ±0.2 PV.

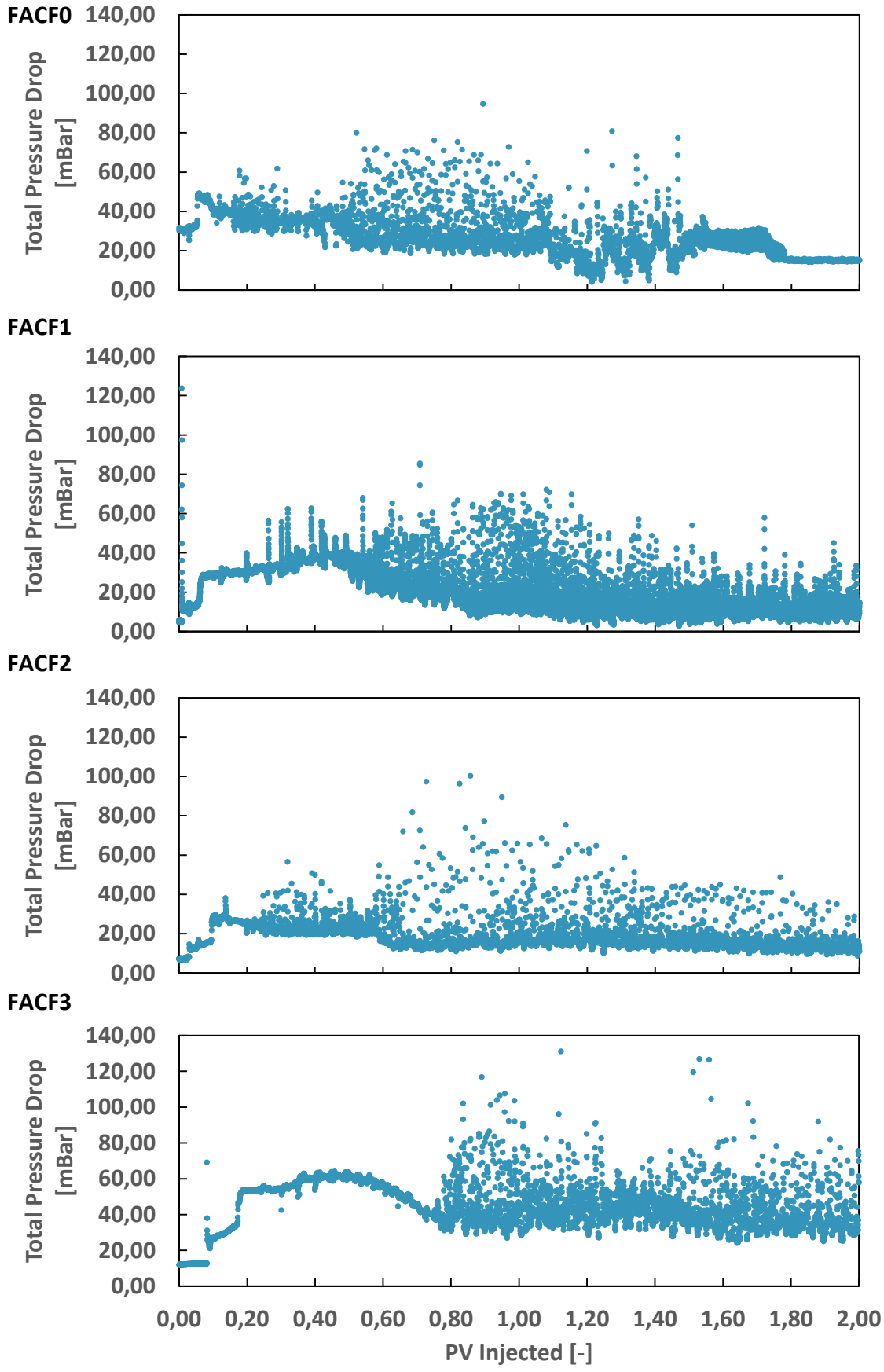

Figure 24: Total pressure drop as function of total PV injected for all FACF core-floods. In all experiments, a foam quality of 57.5% was maintained. For experiment FACF3, a mixing tee was utilized to pre-generate foam prior to entering the core

CT images and saturation profiles

The CT images for both experiments, FACF1 and FACF2 taken during the drive co-injection stages, show high spread out of the oil bank (figure 25 and 26). In comparison to the oil bank shape at the end of surfactant slug injection (figure 22 and 24), with the ones at the beginning of co-injection, the oil bank is still visible with its leading edge traveling faster away from the inlet than the trailing edge. In fact, during FACF2, the CT image shows that some of the oil in the leading edge have already exited the core. The bottom most part of the core-flood in both cases was better swept than the upper most part of the core. That is shown by the higher oil saturation reflected on the images in the upper section. This is evident from the gravity under riding tongue that can be identified in CT images taken at 4.07 PV and 6.26 PV injected respectively for FACF1 and 2. Residual oil to drive co-injection (S_{or_CF}) estimated values based on CT responses are 0.20±0.06 and 0.21±0.03 for FACF1 and FACF2 respectively.

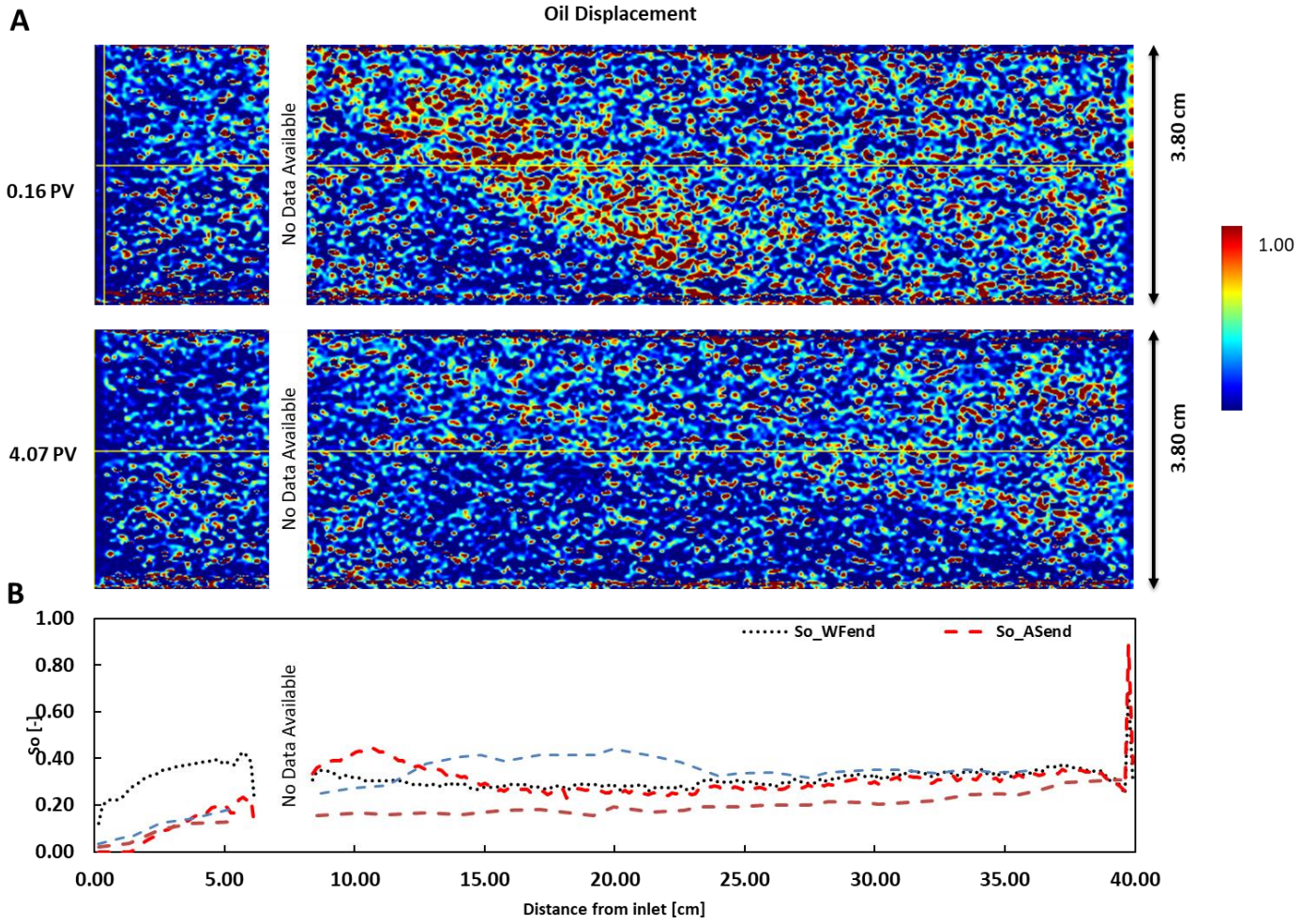

Figure 25: CT images and oil saturation profiles for the co-injection of surfactant drive solution with N_2 in FACF1

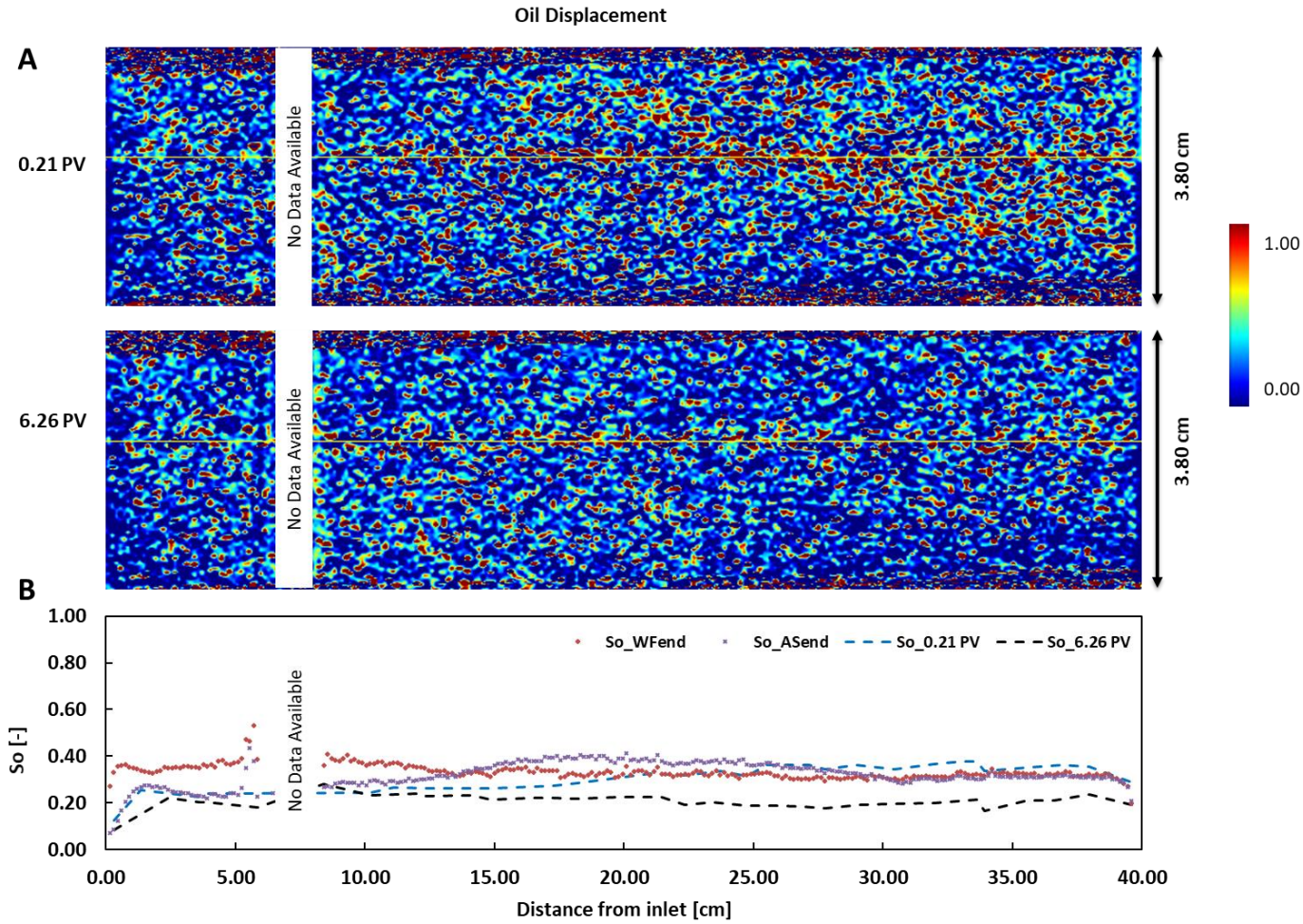

Figure 26: CT images and oil saturation profiles for co-injection of surfactant drive solution with N_2 in FACF2

Gas saturation profiles

The gas saturation profiles during surfactant drive co-injection are shown in figure 27 and 28. The saturation of gas shows a slight increase at the inlet as the co-injection process is initiated, then it follows a constant trend with a relatively low value until the end of the co-injection phase. Gas breakthrough in both experiments occurred after 0.48±0.20 PV (FACF1) and 0.58±0.20 PV (FACF2) of co-injection. An indication of foam generation would be a sudden increase in S_g as the co-injection process is continued. That is due to the fact that equally divided gas phase across a cross-sectional area causes an increase in S_g over that area. In addition, the increase in pressure drop due to the formation of foam could be attributed to the increase in apparent viscosity (equation 6).

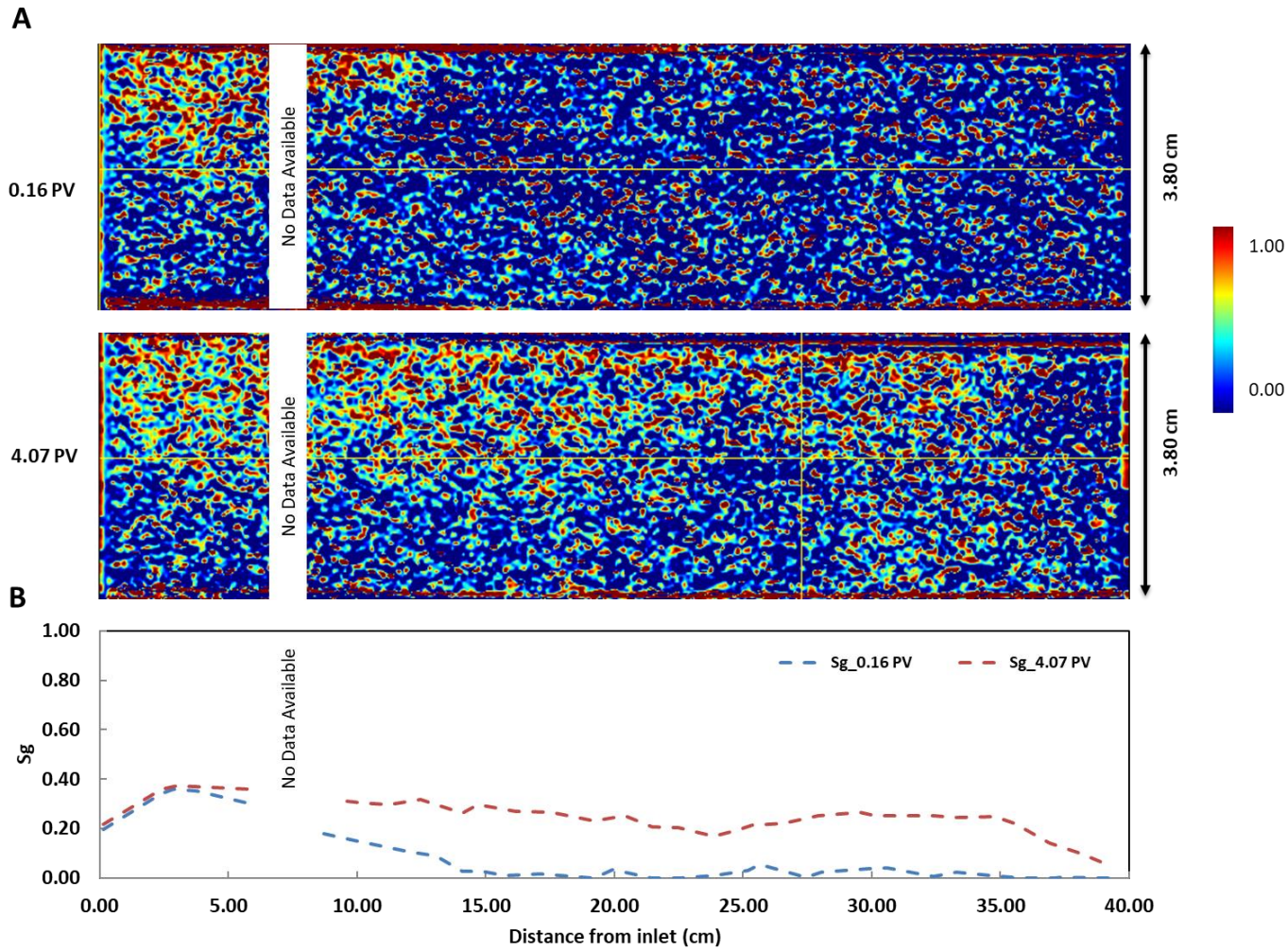

Figure 27: CT images and gas saturation profiles for the co-injection process in FACF1

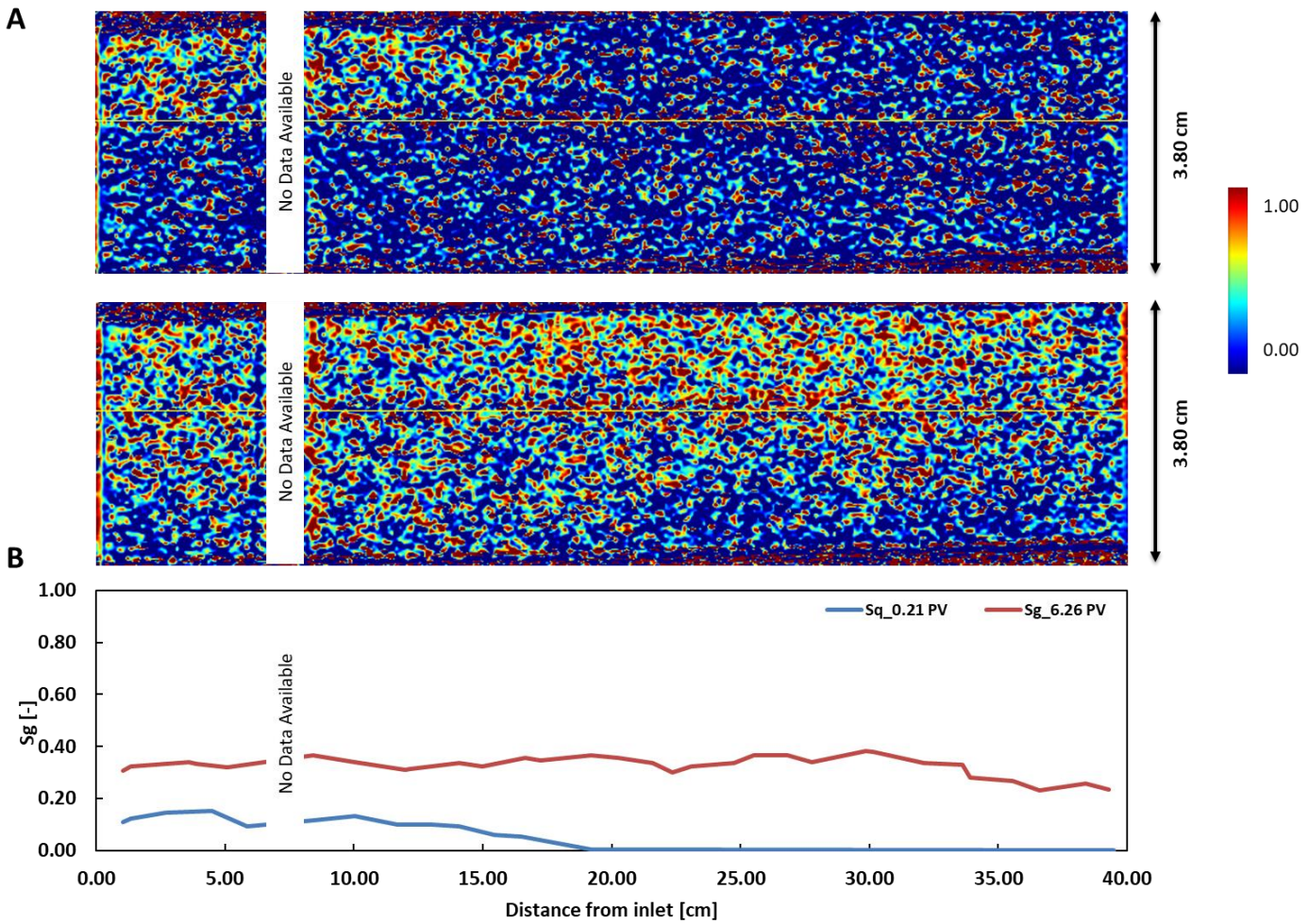

Figure 28: FAFC2 - (A) CT images, (B) Saturation profiles during surfactant drive co-injection

Oil recovery profiles

Figure 29 shows the cumulative oil recovery plot during the surfactant drive co-injection phase for FACF1, FACF2 and FACF3. In both FACF1 and FACF2, the oil breakthrough is seen after 0.17±0.01 and 0.13±0.01 PV of co-injection. That is shown by the quick increase in recovery factor in the early stages of co-injection. Then, for both experiments, the recovery factor starts increasing gradually as oil is being produced. For, FACF3, oil breakthrough was observed relatively later than the previous experiments (at 0.20±0.01 PV). Then, recovery factor increases in the same trend as clean oil is being produced until 0.75 ±0.20 PV, where the gradual increase in recovery tends to flatten down slowly. This is an indication of the emulsified oil that has been produced. It continues this slight increasing trend until no further oil is produced after 1.32 ±0.20 PV of co-injection.

Comparing the three experiments together, it is observed that in both FACF1 and FACF2, production of oil started earlier. The sharp production of all of the oil in relatively short time is shown in FACF2. The recovery profile corresponding to FACF1 exhibits a lower oil production rate compared to FACF2. This is most likely due to the presence of more stable foam front compared to FACF2. In FACF1, no oil was produced after 1.20±0.20 PV of co-injection. In the last experiment, FACF3, it is seen that production started at a relatively later stage than the previous two, with a similar recovery slope as in FACF1 and FACF2. The similarity in the slope is attributed to the shape of the oil bank formed during the surfactant slug injection as shown in the CT images (figure 23 and 24). The shape of oil bank explains why oil was being produced even after gas breakthrough. Initially, oil accumulated at the lower part of the core gets produced, and as foam propagates, it displaces the remaining mobilized oil in the mid-section and top. When gas breakthrough happens, a considerable amount of mobilized oil is left, and gets produced as the co-injection continued. The associated recovery factors resulting from the co-injection phase compared to OIIP is 16±3%, 15±3% and 22±3% for FACF1, FACF2 and FACF3 respectively.

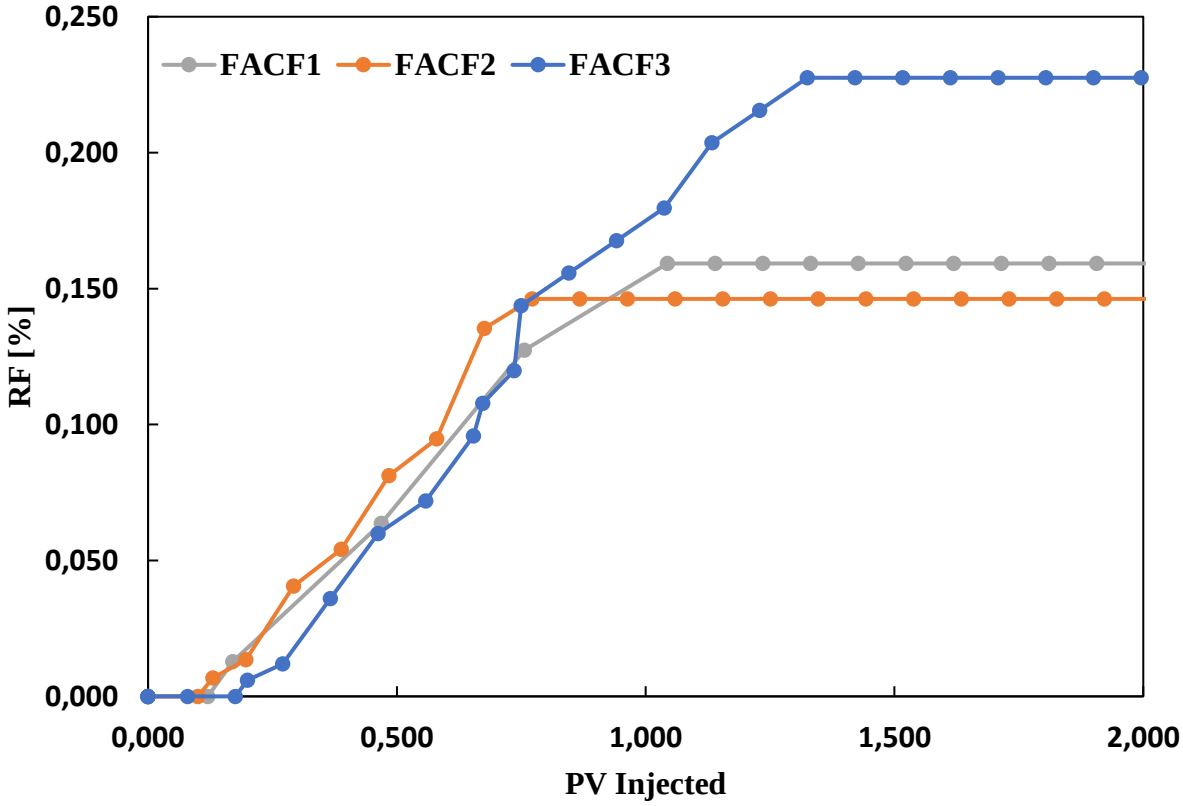

Figure 29: Oil recovery profiles during the surfactant drive co-injection process

5. Summary

In this study, multiple tests and core-flooding experiments were conducted. Starting from surfactant stability in brine, that revealed precipitation will occur in the presence of divalent ions in the original seawater injection brine composition. The results of the surfactant stability tests showed that by removing Mg+ and Ca+ from the synthetic brine composition the surfactant solution did not yield any precipitation of ……. Secondly, three salinity scan tests were performed. The first two tests with two different surfactants supplied by the sponsors. The tests showed that surfactant (A) can be better used as an o/w IFT lowering agent than the other surfactant. In addition, by measuring the oil and water fractions solubilized in the micro-emulsion, the o/micro-emulsion and w/micro-emulsion IFT values were estimated. It showed that the optimum salinity region is between 1.50 wt% and 1.75 wt% NaCl+KCl for surfactant A slug solution. Since two FACF core-flood experiments are carried out with the assistant of a medical CT-scanner, 20 wt% of 1-iododecane was added to the crude oil to enhance the CT response. It was important to test its influence on the salinity scan. Therefore, another salinity scan test was performed using surfactant A and varying NaCl+KCl concentrations with fixed volume of Na_2SO_4, NaHCO3 and sec-butanol. Crude oil with 20wt% 1-idodecane was added to the solutions. The identified range of lowest o/w IFT was the same as in the case where no dopant was used. From this test, it was decided to perform two full EOR FACF experiments at under-optimum salinity conditions, and two at optimum conditions. Next, bulk foam tests were done to evaluate the surfactants ability to generate stable and strong foam in absence and presence of crude oil. Again, both surfactant A and B were assessed on their foaming capabilities in bulk. It was concluded that surfactant B was going to be used as a drive solution because of its better foaming characteristics. Subsequently, a so-called foam quality scan was conducted in absence of oil in Bentheimer sandstone using the surfactant B drive formulation. Then, based on literature, a foam quality of 57.5% was selected for surfactant drive co-injection process on a core at residual oil to waterflooding conditions. Unfortunately, foam was not generated.

Furthermore, in this experimental study four full EOR FACF core-flood experiments were conducted. Two of which at under-optimum salinity conditions and the other two at optimum conditions. In all experiments, crude oil was utilized. For experiments FACF1, 2 and 3 the oil was doped with 20 wt% 1-iododecane. Same procedures were followed throughout the experiments. The only change that was applied to FACF3, is the addition of a mixing tee to pre-generate foam outside the core inlet. The waterflooding process yielded a recovery factor

of 55 ±3%, 61 ±3%, 59 ±3% and 46 ±3% of oil initially in place (OIIP) calculated using material balance equation, respectively for FACF0, FACF1, FACF2 and FACF3. The values for FACF1 and 2 are in agreement and within the accuracy limit of the recovery factors yielded from the processed CT scan data. The first three experiments showed similar values of RF after waterflooding. However, the last experiment showed, relatively, low RF. During the bump flooding in primary drainage and imbibition, pressure reached a steady condition, indicating that residual oil conditions were reached, as well as connate water conditions. Another factor that could contribute in a low RF, is mobility ratio between the displacing fluid and fluid being displaced. The temperature at which the experiment was conducted could have caused the viscosities of both fluids to approach each other. Such conditions could lead to viscous fingering and consequently unfavourable conditions. In FACF1 and FACF2 the CT images with the saturation profiles suggested that the water front was not stable, and it was more likely fingering the oil. With an end-point mobility ratio more than one; upstream phase is more mobile than downstream phase, it confirms the non-stable conditions.

During the slug injection phase, the same behaviour of unfavourable mobility is seen as during waterflooding. However, it was more obvious in this process. Many factors could attribute to this unfavourable condition. Viscosity, density an temperature are critical elements that affect the flow conditions.

The drive solution co-injection phase showed different behaviour in the first three experiments compared to the last one with the mixing tee. In order to judge whether foam was generated or not, total pressure drop data, CT images and gas breakthrough times have to be studied together. For FACF0, 1 and 2, total pressure drop data showed an increase as soon as co-injection was initiated. Soon after, the total pressure drop stabilized for a short period of time then started to decline. The gas saturation profiles form the CT response show that in both experiments FACF1 and FACF2, S_g was low and no sudden increase in saturation was observed. Coriolis flow meter data showed that gas breakthrough happened after 0.44 ±0.02 PV, 0.48 ±0.02 PV and 0.58 ±0.02 PV for FACF0, FACF1 and FACF2 respectively. Total pressure drop data with CT images show that weak foam was generated. In addition, the gas breakthrough times does not agree with the literature values of typical free gas breakthrough in porous media which is estimated to be below 0.30 PV (Hua Guo, 2011) (Janssen, et al., 2018). On the other hand, in FACF3, the pre-generated foam by utilization of the mixing tee, showed multiple features in the total pressure drop data. Started with a spike increase as the co-injection started, then remained steady for a short period. Afterwards, it started increasing again as foam started to

propagate. The relatively significant delay in gas breakthrough is also a good sign that foam was generated and it was stable enough to propagate through porous media. Gas broke through after 0.80 ±0.02 PV. Due to the fact that in both FACF3 and FACF1, same surfactant slug composition was used, and the only variable was adding the mixing tee, we can conclude that the drive foam strength has a bigger impact of the FACF efficiency than its surfactant slug salinity. By looking at the yielded recovery factors after the co-injection phase, it shows that in FACF3 the oil recovery improved by approximately 20%, in comparison to the other experiments.

6. Conclusion

An experimental study approach was followed to examine Foam-Assisted Chemical Flooding as an effective enhanced oil recovery (EOR) technique at reservoir conditions of 90±1°C and 20 bar back pressure. Surfactant stability tests in synthetic brine, bulk foam experiments and several phase behaviour scans were carried out to specify and optimize the synthetic reservoir brine, surfactant slug and surfactant drive formulations. Core-flood experiments at reservoir conditions of 90±1°C and 20 bar back pressure, with and without the assistance of a medical CT scanner were conducted to assess the impact of surfactant slug salinity and drive foam strength on the efficiency of FACF process. These experiments include the injection of a surfactant slug at (under-) optimum salinity conditions in a sandstone core already brought to residual oil saturation to waterflood before co-injecting a surfactant drive formulation with N_2 for foam generation. In one experiment foam was pre-generated prior to injection in the sandstone core. The following conclusions can be drawn from this study:

- The surfactants studied are not stable in synthetic reservoir formation water, when mixed together and placed under temperature of 90±1°C, complexes were formed due to reaction between surfactant and divalent ions, and subsequently caused precipitations. By removing the divalent ions present in Mg^{+2} and Ca^{+2}, surfactants were stable in the model synthetic solution with no precipitations.
- Surfactant B showed good qualities in terms of foam generation and stability in bulk compared to surfactant A in absence of crude oil. It proved to be a better foaming agent to be utilized in the drive co-injection. On the other hand, surfactant A, was able to reduce the o/w IFT more effectively during the phase behaviour study. A clear distinct micro-emulsion was seen in the tubes with surfactant A, while nothing was seen on the other tubes for surfactant B. The optimum salinity condition was achieved in the range from 1.50 wt% to 1.75 wt% NaCl+KCl for the final surfactant A slug composition.
- The salinity of the surfactant slug affected the shape of oil bank formed during the surfactant slug injection. At optimum conditions, the oil bank had more stable front than at under optimum conditions. This was seen from the CT images taken during the surfactant slug injection and at the end of the injection phase. As of the clean oil to emulsified oil ratio, the effect was almost negligible between optimum and under-optimum conditions.
- For the foaming agent, surfactant B, generating foam in situ in presence of oil seemed very challenging. As the crude oil assessed is very detrimental to the stability of foam

and favours its decay, in situ foam generation trials were able to generate week and unstable foam. However, by pre-generating foam outside the sandstone core, foam was stable enough to enter the core and displace the oil efficiently. In fact, in terms of oil recovery, drive foam strength has a bigger impact on FACF efficiency than its surfactant slug salinity.

- By applying FACF EOR technique the yielded RF were calculated to be 70±5 %, 77±5 %, 73±5 % and 80±5 % OIIP for FACF0, FACF1, FACF2 and FACF3.

After this experimental study, a few recommendations are suggested:

- Use the experimental data as input in a modelling study to estimate Brooks-Corey components n_o and n_w so that it is possible to estimate the relative permeability values during the surfactant slug injection. This will confirm quantitatively whether the mobility conditions are unfavourable or not.
- Theoretically, during water flooding and surfactant slug flooding, the fronts were not that stable. For waterflooding, end-point mobility ratios were estimated using relative end-point permeability values, and it yielded values above one, meaning unfavourable mobility conditions existed. It is recommended to add a polymer to the brine and surfactant slug in order to increase its viscosity. With that, it is ensured, depending on how much polymer is added, that the viscosity of the displacing fluid is higher than that of the fluid being displaced, lowering the mobility ratio, and consequently switching the conditions towards the favourable side.

References

A.R. Awan. R. Teigland, J. K., 2008. *A Survey of North Sea Enhanced-Oil-Recovery Projects Initiated During the Years 1975 to 2005.* Tulsa, SPE.

Al Saadi, F., Wolf, K.-H. & Van Kruijsdijk, 2018. *Oil Bank Build Up: An Experimental Approach,* Muscat, Oman: SPE.

Darcy, 1856. *Les fontaines publiques de la ville de Dijon: exposition et application.Victor Dalmont.* , s.l.: s.n.

Falls, A. H. et al., 1988. *Development of a Mechanistic Foam Simulator: The Population Balance and Generation by Snap-Off,* s.l.: SPE.

Falls, A. H., Musters, J. J. & Ratulowski, J., 1980. *The Apparent Viscosity of Foams in Homogeneous Bead Packs,* s.l.: SPE.

Guo, H., Faber, R., Buijse, M. & Zitha, P., 2011. *A Novel Alkaline-Surfactant-Foam EOR process,* Kuala Lumpur, Malaysia: SPE.

Hirasaki, G. J., 1989. *A review of The Steam Foam Process Mechanisms,* s.l.: SPE.

Hosseini-Nasab, S. M. & Zitha, P., 2015. *Systematic Phase Behaviour Study And Foam Stability Analysis For Optimal Alkaline/Surfactant/Foam Enhanced Oil Recovery,* Dresden, Germany: European Symposium on Improved Oil Recovery.

Hu Guo, M. D. W. F. W. G. Y. Z. Y. W. Y. Y. L., 2017. Proper Use of Capillary Number in Chemical Flooding. *Journal of Chemistry,* Volume 2017, Article ID 4307368, p. 11.

Hua Guo, R. F. M. B. P. L. Z., 2011. *A Novel Alkaline-Surfactant-Foam EOR Process.* Kuala Lumpur, SPE.

International Energy Agency, 2018. *Market Report Series - Oil 2018,* Houston: International Energy Agency.

Janssen, M., Zitha, P. & Pilus, R., 2018. *Oil Recovery by Alkaline-Surfactant-Foam (ASF) Flooding: Effect of Drive Foam Quality on Oil Bank Propagation,* Tulsa, Oklahoma, USA: SPE.

Janssen, M., Zitha, P. & Plius, R., 2018. *Oil Recovery by Alkaline-Surfactant-Foam (ASF) Flooding: Effect of Drive Foam Quality on Oil Bank Propagation*, Tulsa, Oklahoma, USA: SPE.

Kam, S. I. & Rossen, W. R., 2003. *A Model for faom generation in homogeneous porous media,* s.l.: SPE.

Kemp, A., 2017. *Petronas to spend over US$2 Billion On EOR Project,* Edinburgh, Schotland: NEWSBASE.

Li, R. F. et al., 2010. Foam Mobility Control for Surfactant Enhanced Oil Recovery. *SPE Journal,* p. 934.

Mayank Srivastava, J. Z. Q. P. N. G. A. P., 2009. *A Systematic Study of Alkaline-Surfactant-Gas Injection as an EOR Technique.* New Orleans, SPE.

OPEC, 2018. *OPEC Monthly Oil Market Report - 13 August,* Vienna, Austria: OPEC.

Pal, S., Mushtaq, M., Banat, F. & Al Sumaiti, A., 2017. *Review o fsurfactant-assisted chemical enhanced oil recovery for carbonate reservoirs: challenges and future perspectives,* Abu Dhabi, UAE: Department of Petroleum Engineering, Khalifa University of Science and Technology.

Pal, S., Mushtaq, M., Banat, F. & Al Sumaiti, A. M., 2017. *Review of surfactant-assisted chemical enhanced oil recovery for carbonate reservoirs: challenges and future perspectives,* Abu Dhabi, UAE: Department of Petroleum Engineering, Khalifa University of Science and Technology.

Patzek, T. W., 1996. *Field Applicatons of Steam Foam for Mobility Improvement and Profile Control,* s.l.: SPE.

Peksa, A. E., Wolf, K.-H. & Zitha, P., 2015. Bentheimer sandstone revisited for experimental purposes. *Marine and Petroleum Geology,* Volume 67, pp. 701-719.

Rossen, W. R., 1996. *Foams in Enhanced Oil Recovery.* New York: Marcel Dekker.

Rouhi Farajzadeh, A. A. H. B. P. L. Z., 2009. Comparative Study of CO2 and N2 Foams in Porous Media at Low and High Pressure - Temeratures. *American Chemical Society,* Issue 48.

Samsudin, N. Y., Husain, D., Hamdan, M. K. & Bhd, C. S., 2005. *Enhanced Oil Recovery in Malaysia: Making It a Reality*, Kuala Lumpur, Malaysia: SPE.

Schramm, L. L., 1994. *Foam Sensitivity to Crude Oil in Porous Media*, Washington, DC, USA: American Chemical Society.

Sheng, J. J., 2011. *Modern Chemical Enhanced Oil Recovery Theory and Practice.* Oxford, UK: Gulf Professional Publishing.

Sheng, J. J., 2011. *Modern Chemical Enhanced Oil Recovery: Theory and Practic.* s.l.:Gulf Professional Publishing.

Sheng, J. J., 2013. *Enhanced Oil Recovery Field Case Studies.* 1 ed. s.l.:Gulf Professional Publishing.

Shupe, R. D., 1981. *Chemical Stability o fPolyacrylamide Polymers*, s.l.: SPE.

Simjoo, M., 2012. *Immischible Foam for Enhancing Oil Recovery*, Delft, Netherlands: TU Delft.

Southwick, J. G. et al., 2018. *Surfactant Flooding in Offshore Environments*, Tulsa, Oklahoma, USA: SPE.

Srivastava, M., Zhang, J., Nguyen, Q. & Pope, G., 2009. *A Systematic Study of Alkaline-Surfactant-Gas Injection as an EOR Technique*, New Orleans, Louisiana, USA: SPE.

Zitha, P. et al., 2018. *SPE.* [Online]
Available at: https://www.spe.org/industry/increasing-hydrocarbon-recovery-factors.php
[Accessed 28 08 2018].